DANISH METEOROLOGICAL INSTITUTE

—— SCIENTIFIC REPORT ——

00-11

Diagnosis of visibility in DMI-HIRLAM

Claus Petersen
Niels Woetmann Nielsen

DMI

Diagnosis of visibility in DMI-HIRLAM

Claus Petersen and Niels Woetmann Nielsen
Danish Meteorological Institute

1. Introduction

It is of particular importance to predict extreme weather events as accurately as possible. State of the art numerical weather prediction models, like HIRLAM, have proven to be able to predict extremes of wind, temperature, surface pressure and precipitation with a high degree of success. Visibility could be added to the list, because accurate prediction of low visibility, i.e. fog, is of great concern for land, sea and air traffic.

However, visibility has not been widely included as a prognostic or diagnostic parameter in operational numerical weather prediction models. The main reason is that visibility in a rather complex way depends on parameters like relative humidity, cloud water, precipitation, soil moisture, vegetation, snow cover and aerosol concentration. Furthermore dust, snow drift, sea spray and smoke can occasionally reduce the visibility.

The present report contains a description of the implementation of visibility as a diagnostic parameter in DMI-HIRLAM. Aerosols are not included in the HIRLAM model. Therefore it is impossible to take the effect of aerosols on visibility directly into account. The parameterization of visibility developed for DMI-HIRLAM is to some extent based on statistics. The parameterization has been developed in three steps.

In the first step an empirical, statistically based function is derived. This function relates visibility to observations of total cloud cover, solar zenith angle, temperature, humidity (dew point temperature) at screen level and wind speed and wind direction at 10 m height. The function is optimized by fitting the calculated visibility to observed visibility at available synop stations in Denmark for a period of two years. By this procedure the visibility is calculated from the parameters in the synop report listed above, and the result is then compared with the reported visibility. It has not been possible to make a fit of calculated versus observed visibility without considerable scatter. This is mainly due to uncertainties in the measured dew point depression (difference between temperature and dew point temperature) and its localness (site dependency) combined with subjective estimates of visibility.

In the second step the visibility function derived in step one is implemented in the 1-dimensional version of DMI-HIRLAM and tested on idealized cases. The model contains additional information that is not present in the synop reports, for example surface temperature, rain and snow intensity, temperature, specific humidity and cloud water at the lowest model level. Therefore, the visibility function is modified to take into account these additional parameters. However, for the time being cloud water is not included, because it has been found that the model has a tendency to predict too high amounts of cloud water in the boundary layer close to the ground.

Finally, in step three the modified visibility function developed in step two is implemented in the 3-dimensional DMI-HIRLAM and tested on selected cases. The case

studies are followed by verification against observations (obs-verification) of 3 and 6 hours visibility forecasts from daily analyses at 00 UTC for April, August, November and December 1999.

The theoretical basis for calculation of visibility and the strategy followed in the development of a diagnostic visibility function for DMI-HIRLAM is presented in section 2. A statistical analysis of 3 hourly visibility observations from the Danish synop stations for a period of 2 years is presented in section 3. The statistical analysis is used as guidance for the development of the empirical visibility function described in section 4. Results of 1-dimensional DMI-HIRLAM experiments with visibility included as a diagnostic variable is presented in section 5. A modification of the diagnostic stability function, taking into account additional information available in DMI-HIRLAM such as rain and snow intensity is presented in section 6. The modified visibility function is implemented in the 3-dimensional DMI-HIRLAM and results from selected cases are discussed in section 7. In section 8 obs-verification results for visibility are presented for April, August, November and December 1999. Finally, section 9 contains a brief summary and a discussion of limitations of the present calculation of visibility and suggestions for further improvement of the visibility-calculation in the HIRLAM model.

2. Fog and visibility

The visibility in the atmosphere is reduced mainly because of scattering of light. The scattering occurs on air molecules, aerosols (including dust, smoke and salt particles), cloud drops and precipitation particles. It is a common experience that the visibility drops dramatically from cloud free air to clouds. At the surface the latter significantly changes the visibility if fog forms locally or is advected from a nearby source.

2.1. Fog

Fog (cloudy air) forms in the atmosphere if its state changes from q, T, p to $q^{'}, T^{'}, p^{'}$ such that $q^{'} = q_s(T^{'})$, where $q_s(T^{'})$ is the saturation specific humidity at temperature $T^{'}$ and pressure $p^{'}$. The effect of changing pressure is usually small. Therefore the processes frequently transforming the atmospheric state from unsaturation to saturation are moistening and cooling. Also drying and cooling can lead to saturation if the cooling dominates, and likewise moistening and warming can generate fog if the moistening dominates.

In an unsaturated environment the moisture of the air changes by the following processes: Turbulent mixing of air masses with different moisture content, turbulent and molecular transport of moisture to or from the underlying surface, and evaporation from precipitation falling through the air. If the air is saturated or supersaturated condensation takes place at a speed that keeps the atmospheric state near saturation. The visibility of the air decreases with increasing amount of condensate suspended in the air (see subsection 2.2).

Heating and cooling of the atmospheric state can occur as the result of: turbulent mixing of air masses with different temperature, turbulent and molecular sensible heat flux to or from the underlying surface, radiative cooling at the surface and radiative flux divergence in the atmosphere.

Fog has been classified in terms of the processes listed above. The main classes are

2

- Advection fog

- Frontal fog

- Radiation fog

Turbulent mixing dominates in advection fog. The latter typical forms when cold and moist air flows over a warm sea or when warm and moist air flows over a cold sea (or a cold and wet land surface). If the horizontal surface pressure gradient is week the turbulent mixing may die out and in absence of radiative cooling prevent formation of fog in the latter case.

Frontal fog typically forms as a result of moistening of the subfrontal cool and unsaturated air by evaporation from precipitation particles falling from the frontal clouds aloft.

Radiative cooling at the surface and in the air (in case of radiative flux divergence) dominates in radiation fog. Radiation fog may form initially above the surface as the result of cooling due to radiative flux divergence. Often, and in particular if the surface is wet, radiation fog first forms at the surface and grows in depth if the radiative cooling continues. After the initial formation of fog at the surface the maximum in radiative cooling becomes displaced from the surface to the top of the fog layer.

Vegetation has a significantly lover heat capacity than bare soil. Consequently vegetation cools faster than bare soil and saturation first occurs at the vegetation. In this phase turbulence and molecular interactions transport moisture from the air and the wet soil to the vegetation, where it condenses as dew or rime. The radiative cooling may continue without formation of fog until the air at the surface becomes saturated. If the air and soil are sufficiently dry radiative cooling at the surface may not persist long enough to saturate the air. The latter situation is not uncommon over land in summer in middle and high latitudes. In these conditions it is often observed that radiation fog only forms locally over patches of wet land and in particular in combination with a local minimum in terrain height. More generally, radiation fog typically forms over land in clear nights with calm winds.

A review of theoretical work on fog is presented in (Cotton and Anthes, 1989).

2.2. Visibility

Visibility is a measurement of how far away an object can bee seen. This depends of the luminance of the object and the physical state of the atmosphere. The luminance is defined by the relation

$$\frac{I(x_{obs})}{I_0} = \exp(-\int_0^{x_{obs}} \beta(x)dx) \tag{1}$$

where I_0 is the luminance of the object, $I(x_{obs})$ is the luminance that reaches an observer a distance x_{obs} from the object and β is the extinction coefficient which includes absorption and scattering of light. For cloud water absorption can be neglected. The relation 1 is the solution to the equation

$$\frac{DI}{Dx} = -\beta(x)I \tag{2}$$

3

If β is a constant equation (1) reduces to

$$VIS = -\frac{\ln(0.02)}{\beta} \qquad (3)$$

The ratio $I(x_{obs})/I_0$ is here defined as 0.02, which means that only 2 percent of the light from the object is received at the distance $VIS = x_{obs}$ from the object. The meteorological optical range (MOR) is sometimes defined as 0.05 instead of 0.02. The unit of visibility (VIS in (3)) is in km. The extinction coefficient has been determined empirically (Kunkel, 1984). It is primarily a function of the concentration of hydrometeors in the air. Table 1 shows proposed values of extinction coefficients for the four most important hydrometeors in the atmosphere. Note that C in Table 1 is the density of hydrometeors in gm^{-3}.

Table 1: Extinction coefficients as proposed by (Kunkel, 1984)

Hydrometeor	relationship
Cloud liquid water, fog	$\beta = 144.7C^{0.88}$
Rain	$\beta = 1.1C^{0.75}$
Cloud ice	$\beta = 163.9C^{1.00}$
Snow	$\beta = 10.4C^{0.78}$

3. A statistical analysis of observed visibility

To get an idea of how visibility depends on other parameters available in the synop report the frequency of visibility observations in selected intervals (classes) as function of other synoptic parameters has been calculated. The calculation is based on 3-hourly observations from 29 Danish synop stations shown in Figure 1 and is done for a period of 2 years (August 1997 to July 1999). Observations with errors, including incomplete reports with one or more parameters missing, have not been used. Total cloud cover, which is reported in octals (0 to 8) and as 9 if the total cover can not be observed, is used with 9 interpreted as 8. After the error control the total number of reports in the investigation amounts to 139337.

Figure 2 shows the number of visibility observations in 5 km intervals ranging from [0,5[km to [100,∞[km. It is clear from this figure that the majority of the observations have a visibility below 25 km. In the first 5 intervals the number of observations are in the range from 19000 to 23000, but less than 2000 observations have a visibility higher than 60 km

Low visibility is of greater concern than very high visibility. Therefore the emphasis here is on low visibility ($\leq 1000\,m$).
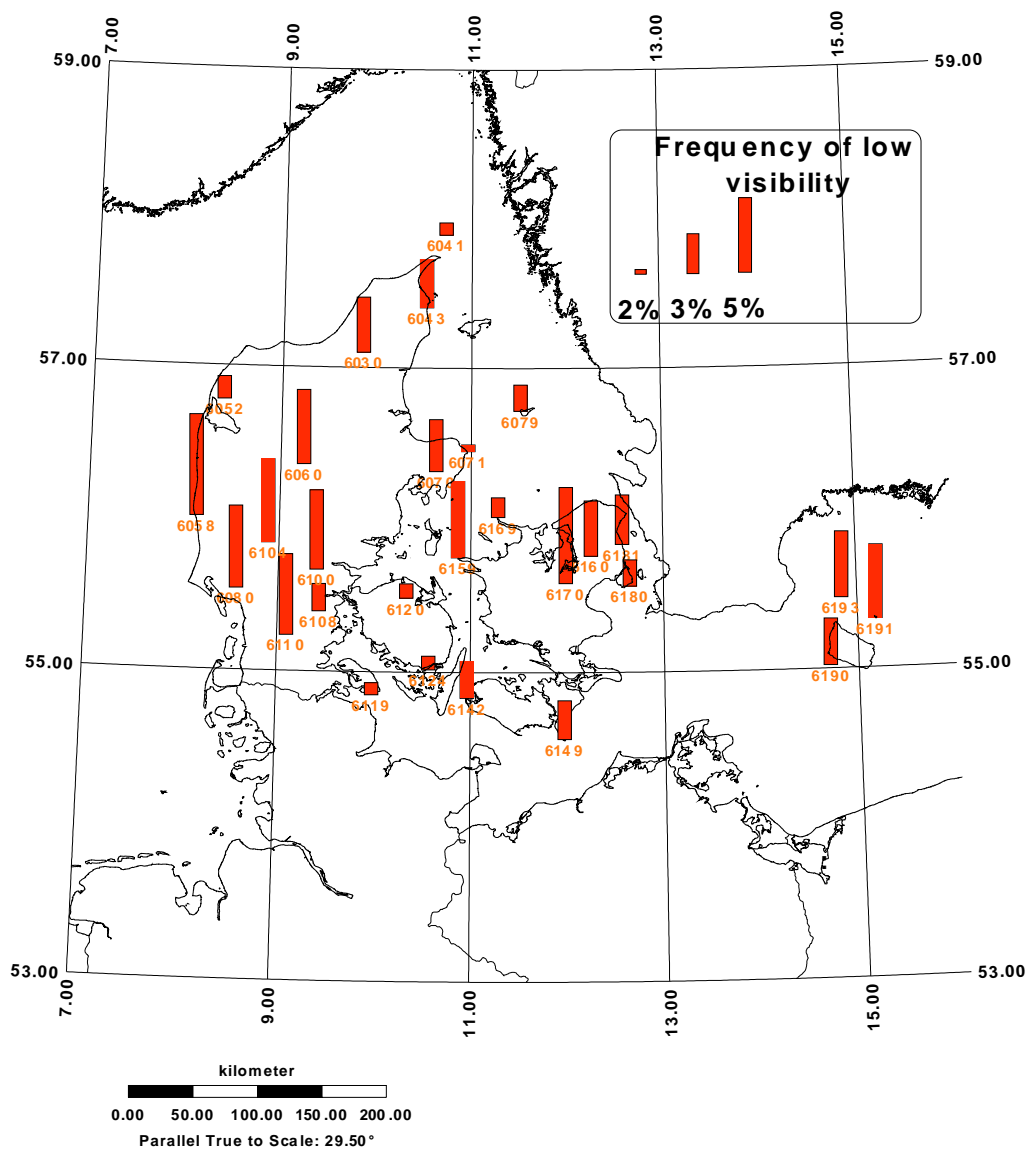
Figure 1: Location of the Danish synop stations from which observations have been used. The vertical bars measure the relative frequency of fog (visibility below 1000 m) .

The frequency of low visibility at the selected 29 Danish synop stations is shown in Figure 1. The relative number, i.e. the number of observations with low visibility normalized by the total number is shown for each station. The relative frequency varies from about 2 to 5 % with a clear tendency for the land stations to have higher frequency of low visibility than the coastal stations. The peak frequencies occur at land stations in southern Jutland. Radiation fog is expected to occur more frequently at land stations than at coastal stations, because at the latter stations warm advection from the sea more often counteract radiative cooling. Therefore it is likely that radiation fog is the main contributor to the observed difference in the frequency of low visibility shown by Figure 2. Other factors, like soil wetness and height and shape of terrain at the station site may also contribute to the observed variability in frequency of fog.

Radiation fog is expected to have a diurnal variation with a maximum of occurrence in the early morning hours. This is in particular the case in summer, where the radiative cooling period is short compared with the situation in winter. Figure 3 shows the distribution of the relative number of observations with low visibility as function of the time of the day. As expected the minimum frequency (2.4%) is found in the noon to afternoon period and the maximum frequency (5.0%) in the late night and morning hours. The diurnal amplitude is damped by the yearly averaging, and also advection fog, which has no clear diurnal variation and tends to have a maximum in winter and spring contributes to smooth out the diurnal amplitude in Figure 3.

3.1. Dew point depression

Dew point depression (DPD), i.e. temperature minus dew point temperature is expected to be strongly correlated with visibility. This is confirmed by Figure 4, showing the relative number of cases with low visibility for different intervals of DPD from $[0,0.1[$ K in steps of 0.1 K to $[2,\infty[$ K. It is clear from Figure 4 that the relative frequency of low visibility decreases with increasing DPD (as expected). However, the figure also shows that only 17.8% of the observations with DPD ≤ 0.1 K has a visibility below 1000 m. Furthermore, the relative number of observations with low visibility is substantial (8.5%) even at DPD's as high as 0.6 to 0.7 K. Precipitation, in particular snow, undoubtly contributes to the latter, while uncertainty in measurement of DPD may contribute significantly to the former. It probably also plays a role that the measurements of DPD at the synop stations not always are representative for a larger area.

3.2. Wind speed

If radiation fog dominates, low visibility is expected to be more frequent at low wind speeds than at high wind speeds. The reason is firstly that turbulent sensible heat flux in stably stratified air counteracts radiative cooling at the surface, and secondly that the counteracting effect increases with wind speed at a fixed vertical temperature gradient. On the other hand, advection fog forms by turbulent mixing. Hence, if advection fog dominates low visibility is expected to have a peak frequency of occurrence at intermediate (not too low and not too high) wind speeds. Advection fog is common over sea, while radiation fog tends to dominate over land. The latter is apparently confirmed by Figure 5, showing the relative frequency of low visibility as function of wind

6

speed (measured in knot). The figure shows a rapid decrease in the relative frequency of low visibility in the range from 1 to 8 knob. In this range the frequency drops from 12.5% to 3.5%.

3.3. Temperature

Due to sources of moisture (sea, lakes, soil moisture, snow, ice) the air near the surface will always contain water vapor, while advection and sinks of water vapor in the atmosphere keeps the climatological value below saturation. For this reason the probability of cooling to saturations is expected to be high at low temperatures and low at high temperatures. This is confirmed by Figure 6, showing the relative frequency of low visibility as function of temperature together with the absolute number of observations (continuous curve) in each temperature interval. The maximum number of observations of low visibility occurs in the intermediate temperature range from 3 to 6 °C. The relative number of low visibility observations is here as low as 5 to 6%.

3.4. Product of DPD and wind speed

The results presented above indicate that visibility is most strongly correlated with DPD and wind speed, such that low visibility tends to occur at small DPD and low wind speed. The product of DPD and wind speed (DPDW) is very clearly correlated with the frequency of low visibility, as shown in Figure 7. Note that the drop in frequency follows the drop in the absolute number of observations (continuous curve in Figure 7). Thus, the maximum frequency (17%) is observed for DPDW in the interval $[0,1]°C{\cdot}knot$, which also contains the maximum number of observations.
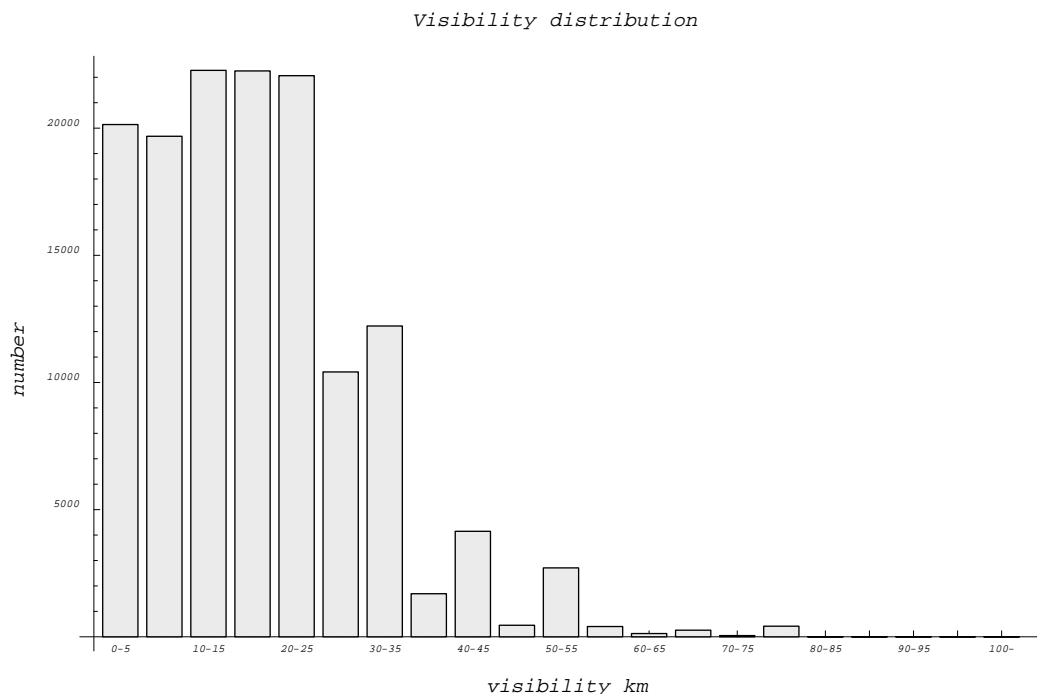

Figure 2: Distribution of visibility observations within 5 km visibility classes.
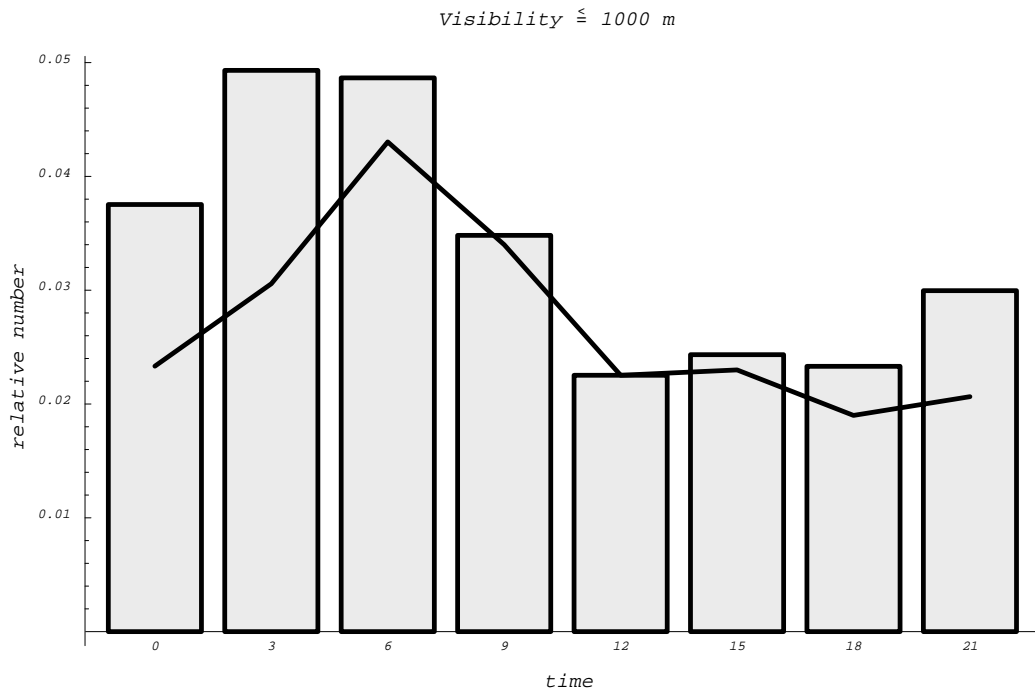
Figure 3: Diurnal relative frequency of fog in 3 hour wide classes. Full curve shows the absolute number of observations.
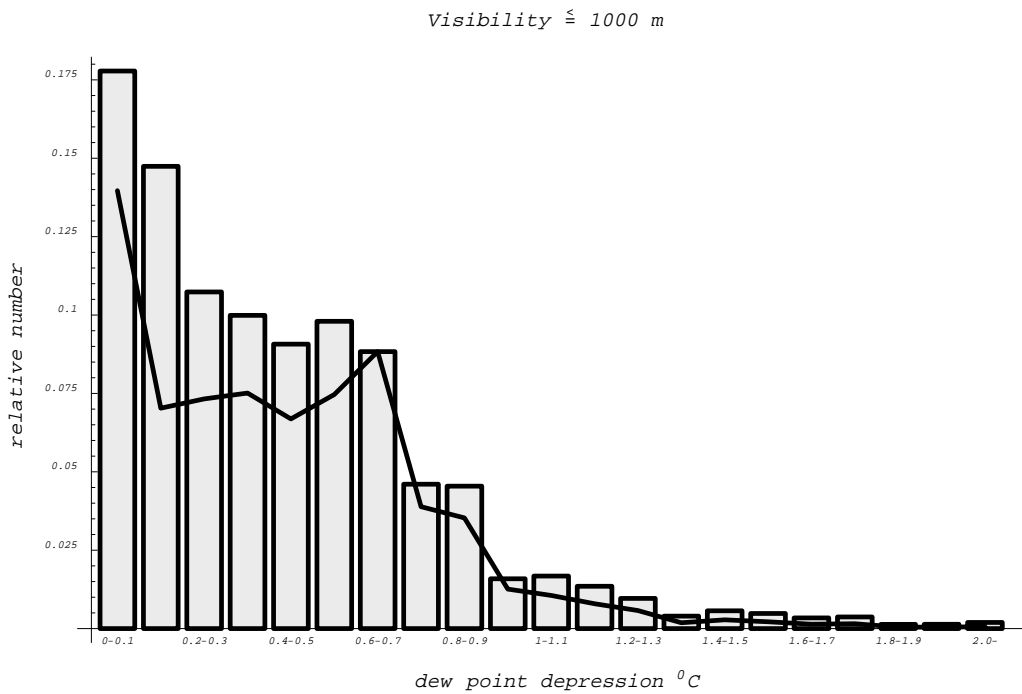

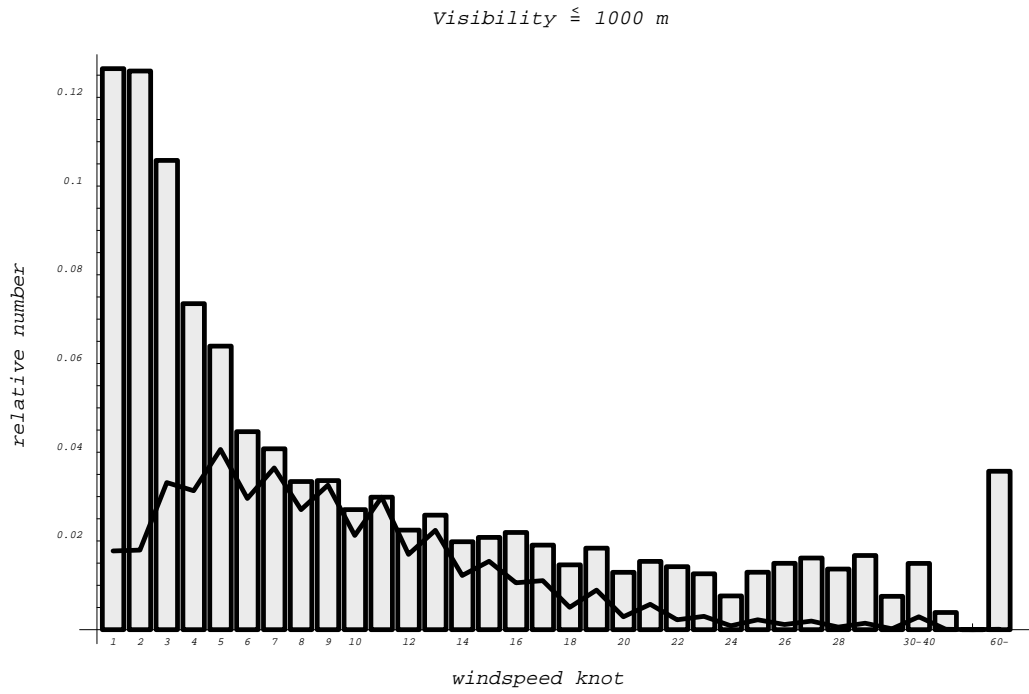Figure 4: Relative frequency of fog in 0.1°C wide classes of DPD. Full curve as in Figure 3.

8

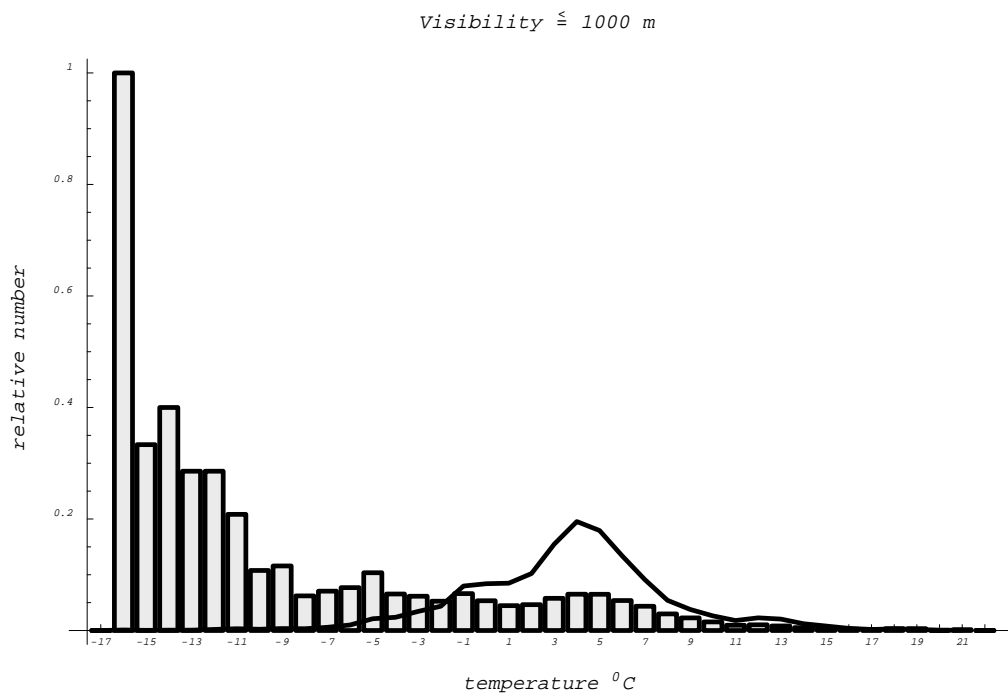Figure 5: Relative frequency of fog in windspeed intervals of 1 knot. Full curve as in Figure 3.

Figure 6: Relative frequency of fog in temperature intervals of 1°C. Full curve as in Figure 3.
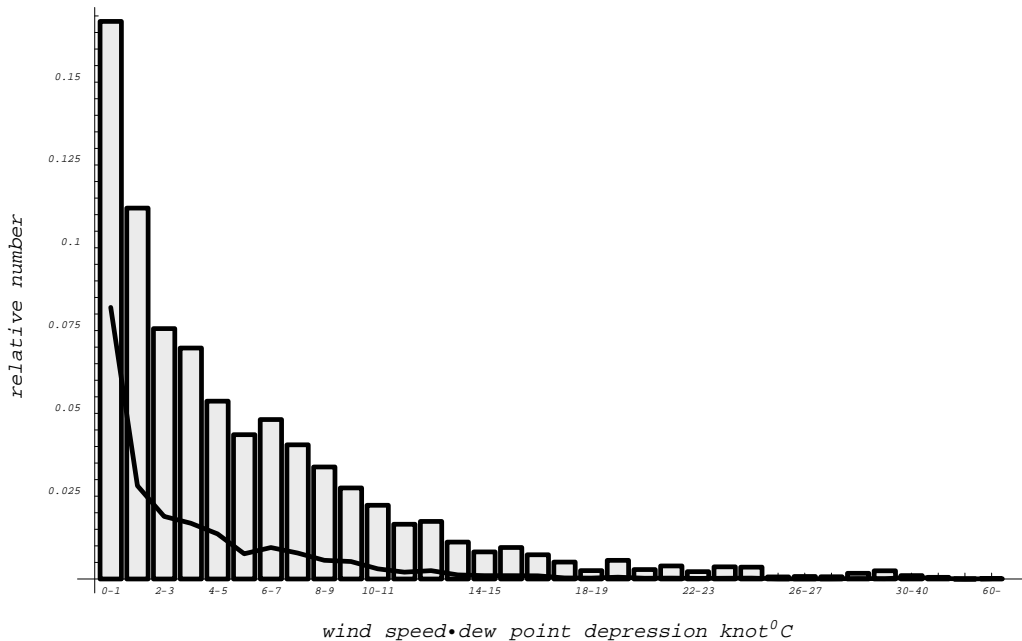
Figure 7: Relative frequency of fog as function of wind speed · dew point in intervals of 1 knot·°. Full curve as in Figure 3

.

4. Development of a diagnostic visibility function

It is not an easy task to develop an empirical relation between visibility and other parameters in the synop report. Part of the difficulty is uncertainty in the measurement of humidity combined with estimates of visibility that in most cases are subjective. Another part of the difficulty is that cloud water measurements are not done. Furthermore, visibility is an integral measurement, representing a large area, while the measurements of temperature, dew point temperature and wind are local.

Following (Kunkel, 1984), the visibility is given by

$$VIS = d \cdot C^{-0.88} \tag{4}$$

In (4) $C = \rho_a \cdot q_c$ is the density of cloud water, ρ_a is the air density (in kgm^{-3}) and q_c is the specific cloud water in gkg^{-1}. In the present report the visibility VIS is calculated in m. Then, according to Table 1 (section 2) the constant d takes the value $d = -1000 \cdot \ln(0.02)/144.7 \simeq 27.0$.

The basic problem in calculating the visibility in equation (4) from other parameters in the synop report is that a pseudo cloud water (PCW) replacing C in (4) has to be estimated from these parameters. The PCW should also include the effect of aerosols and precipitation on visibility. The latter requires measurement of precipitation intensity. From the synop reports only a very inaccurate estimate of precipitation intensity can be obtained, and it has therefore been decided not to take the effect of precipitation into account in the formula developed in this section.

10

It is assumed that PCW can be split into 3 parts, a background contribution σ_{bg}, an aerosol contribution σ_{as} and a cloud water contribution σ_{cw} such that

$$PCW = \sigma_{bg} + \sigma_{as} + \sigma_{cw} \tag{5}$$

The background value represents air without cloud water and with an 'average' aerosol content. It is given the value

$$\sigma_{bg} = 1.8 \cdot 10^{-4} g\,kg^{-1} \tag{6}$$

The variation in aerosol content is parameterized in a very simple way. The content is enhanced and reduced if the wind at 10 m height has a component from south and north, respectively. The amplitude increases with wind speed asymptotically to a constant value and is zero in calm winds. The parameterization takes the form

$$\sigma_{as} = \sigma_{00} \cdot \frac{v}{2+v} \cdot \sin(dd - 90), \tag{7}$$

in which $\sigma_{00} = 0.8 \cdot 10^{-4} g\,kg^{-1}$, and v (in $m\,s^{-1}$) and dd (in degrees with south=180 °) is wind speed and direction at 10 m height. It follows from (6) and (7) that the visibility at a wind speed of for example $5 m\,s^{-1}$ varies from about 75 km in 'clean' air (wind from north) to about 42 km in 'polluted' air (wind from south). The parameterization is developed for Denmark, and is not realistic in regions where "polluted" air is advected by winds from north.

The statistical analysis presented in section 3 is utilized as a guidance in the parameterization of the cloud water contribution σ_{cw} to the visibility. The result is

$$\sigma_{cw} = 0.25\left(1 + \frac{N}{8}\right)\left(1 + \frac{\widehat{dt}}{(1+\widehat{dt})}\right)\exp(-\alpha[(\delta \cdot x(x-x0)+c_2)\cdot\widehat{dt}+\delta c_1 x^2(x-x0)]) \tag{8}$$

Here N is the cloud cover in octals with $N = 9$ interpreted as $N = 8$. The parameter $\widehat{dt}$ is related to the dew point depression at screen level (DPD) and the solar zenith angle (z) and given by

$$\widehat{dt} = \frac{(DPD + c_0)}{(1 - c_3 \cdot cosz)}, \tag{9}$$

with $c_0 = 0.02$ and $c_3 = 1$ (at present). The constant c_0 prevents the visibility from becoming zero if both wind speed and DPD is zero. The constant c_3 could be replaced by a variable for example $c_3 = dmin/dmax$, where $dmin$ and $dmax$ is the minimum and maximum day length, respectively. The latter would prevent $\widehat{dt}$ from becoming infinite in the tropics.

The exponential function in (8) contains 2 terms. The first term is a product of $\widehat{dt}$ and a function of wind speed given by

$$f_1 = \delta \cdot x(x - x_0) + c_2, \tag{10}$$

where $x = (2v + 1)^{1/3}$, $x_0 = (2v_0 + 1)^{1/3}$ and $\delta = \delta_0(1 + \delta_0 x^2)^{-1}$. The constants have the values $v_0 = 3.5\ m\,s^{-1}$, $\delta_0 = 2x_0^{-2}$ and $c_2 = 5$. The term f_1 represents to some extent the correlation between the frequency of low visibility and the product of DPD and

windspeed found in the observations (7). The second term f_2 is a function of wind speed alone and has the form

$$f_2 = 0.2\delta \cdot x^2 (x - x_0).$$ (11)

Finally, the factor α in (8) is a decreasing function of $\widehat{dt}$, given by

$$\alpha = \alpha_0 - \frac{\widehat{dt} \cdot f_a}{(1 + f_a f_b \widehat{dt})},$$ (12)

where $f_a = \alpha_0(1 + 2\alpha_0 \widehat{dt})$, $f_b = \alpha_o^{-1} + 0.15 - 0.2\widehat{dt}(1 + 4/3\widehat{dt})^{-1}$ and $\alpha_0 = 4$. The function α decreases rapidly with $\widehat{dt}$ for small values of $\widehat{dt}$ and has the asymptotic value 0 for $\widehat{dt} \to \infty$

The visibility calculated from wind, temperature, dew point temperature and total cloud cover in the synop report, utilizing equations (4) to (12) has been intercompared with the observed visibility in the same report for a period of 2 years (August 1997 to July 1999) and for 29 Danish synop stations. The results are presented as contingency tables with observed and calculated visibility along the horizontal and vertical axis, respectively.

Tables 2 to 13 show the results for each month of the year. A closer inspection of the tables reveals a clear picture with a too high frequency of 'predicted' visibility in the range from 0 to 5 km and a too low frequency above 10 km. This picture is particularly clear in winter. The diurnal variation at 3 hours intervals of a coresponding statistics for August 1997 to July 1999 is shown in tables 14 to 21. Information about hit rate (h), false alarm (f) and score S defined as $S = 1 - \sqrt{(0.5((1 - h)^2 + f^2))}$ has been extracted from each table. The results for visibility in the range 0 to 5 km (containing the 3 lowest classes) are presented in Figure 8. This figure shows a significant seasonal variation in both hit rate and false alarm. The out-of- phase variation of these statistical parameters gives the lowest and highest scores (S) in summer and winter, respectively.

In summer the typical number of observations with visibility below 5 km is only about 30% of the corresponding number in winter. The statistical uncertainty is therefore higher in summer and is likely to contribute to the lower scores. However, the main reason for the lower scores in summer is believed to be due to a lower representativeness of the local temperature and dew point measurements. The latter is caused by the more scattered occurrence of low visibility (fog) in summer.

5. One-dimensional DMI-HIRLAM case studies with diagnostic calculation of visibility

In the next step the calculation of visibility described in section 4 has been implemented in a 1 dimensional version of DMI-HIRLAM. This intermediate step has been taken because it is more convenient and easier to test if the implementation of visibility and associated changes in code structure has been done correctly in the column version of DMI-HIRLAM.

Table 2: **January 1998 and 1999**

$\frac{obs}{for}$	0-0.4	0.4-1	1-5	5-10	10-25	25-50	50-
0-0.4	74	34	454	297	231	59	14
0.4-1	32	33	402	291	237	58	3
1-5	153	66	1196	1450	1639	370	19
5-10	19	4	114	464	1052	330	14
10-25	2	1	17	257	961	626	79
25-50	1	0	0	12	115	262	80
50-	0	0	0	0	0	0	0

Table 3: **February 1998 and 1999**

$\frac{obs}{for}$	0-0.4	0.4-1	1-5	5-10	10-25	25-50	50-
0-0.4	143	94	610	264	175	35	3
0.4-1	64	49	435	186	137	28	3
1-5	152	124	1340	983	832	216	2
5-10	34	18	337	435	680	188	12
10-25	1	2	127	466	1122	565	61
25-50	0	0	2	45	180	221	18
50-	0	0	0	0	0	0	0

Table 4: **March 1998 and 1999**

$\frac{obs}{for}$	0-0.4	0.4-1	1-5	5-10	10-25	25-50	50-
0-0.4	89	67	443	232	125	24	9
0.4-1	40	36	272	140	89	18	6
1-5	116	99	900	885	888	220	18
5-10	25	23	258	441	804	241	17
10-25	6	7	195	709	1619	740	78
25-50	0	0	9	176	721	746	216
50-	0	0	0	0	0	1	0

Table 5: **April 1998 and 1999**

$\frac{obs}{for}$	0-0.4	0.4-1	1-5	5-10	10-25	25-50	50-
0-0.4	74	55	374	207	114	22	2
0.4-1	25	16	216	158	93	16	1
1-5	99	70	880	825	769	148	9
5-10	25	14	316	491	688	190	8
10-25	10	6	320	799	1444	500	30
25-50	3	0	71	434	910	583	76
50-	0	0	0	1	3	5	3

Table 6: **May 1998 and 1999**

$\frac{obs}{for}$	0-0.4	0.4-1	1-5	5-10	10-25	25-50	50-
0-0.4	27	7	133	137	86	46	2
0.4-1	4	9	85	81	71	16	7
1-5	21	13	294	504	612	252	16
5-10	8	6	113	259	620	267	11
10-25	4	4	130	530	1538	811	82
25-50	1	0	32	463	1815	2049	373
50-	0	0	0	0	6	10	3

Table 7: **June 1998 and 1999**

$\frac{obs}{for}$	0-0.4	0.4-1	1-5	5-10	10-25	25-50	50-
0-0.4	2	10	81	105	81	24	9
0.4-1	6	1	68	81	72	23	6
1-5	19	13	335	553	708	251	21
5-10	4	2	111	322	700	202	19
10-25	1	3	170	581	1748	725	67
25-50	0	0	14	339	1844	1599	301
50-	0	0	0	0	0	0	0

Table 8: **July 1998 and 1999**

$\frac{obs}{for}$	0-0.4	0.4-1	1-5	5-10	10-25	25-50	50-
0-0.4	0	2	37	69	84	35	11
0.4-1	2	1	39	71	65	29	6
1-5	11	13	237	521	825	327	26
5-10	4	4	66	259	793	311	20
10-25	4	0	73	398	1838	846	92
25-50	2	0	5	278	1786	1811	376
50-	0	0	0	0	1	0	2

Table 9: **August 1997 and 1998**

$\frac{obs}{for}$	0-0.4	0.4-1	1-5	5-10	10-25	25-50	50-
0-0.4	6	3	28	29	32	37	9
0.4-1	1	2	25	41	43	26	5
1-5	36	33	284	424	758	423	35
5-10	8	4	131	285	816	389	31
10-25	4	0	135	533	2032	1057	78
25-50	0	0	42	414	2029	1897	338
50-	0	0	0	0	1	1	0

14

Table 10: **September 1997 and 1998**

$\frac{obs}{for}$	0-0.4	0.4-1	1-5	5-10	10-25	25-50	50-
0-0.4	28	8	128	79	37	17	7
0.4-1	20	14	86	69	52	31	8
1-5	110	55	674	741	939	333	39
5-10	16	11	270	443	960	319	25
10-25	7	3	162	750	2066	926	88
25-50	0	0	14	216	1080	963	246
50-	0	0	0	0	0	0	0

Table 11: **October 1997 and 1998**

$\frac{obs}{for}$	0-0.4	0.4-1	1-5	5-10	10-25	25-50	50-
0-0.4	10	9	141	112	93	56	16
0.4-1	11	11	149	93	105	75	5
1-5	37	25	745	837	1118	524	41
5-10	4	6	211	461	1138	469	43
10-25	2	1	48	372	2008	1317	172
25-50	0	0	8	89	701	794	249
50-	0	0	0	0	0	0	0

Table 12: **November 1997 and 1998**

$\frac{obs}{for}$	0-0.4	0.4-1	1-5	5-10	10-25	25-50	50-
0-0.4	75	64	431	164	99	48	3
0.4-1	39	31	420	182	157	34	6
1-5	127	109	1522	1153	1401	362	16
5-10	9	7	233	550	1140	423	18
10-25	1	1	41	350	1402	850	96
25-50	1	0	0	19	106	161	44
50-	0	0	0	0	0	0	0

Table 13: **December 1997 and 1998**

$\frac{obs}{for}$	0-0.4	0.4-1	1-5	5-10	10-25	25-50	50-
0-0.4	161	133	704	313	134	47	5
0.4-1	99	85	597	316	197	32	1
1-5	187	136	1641	1323	1385	296	12
5-10	16	9	157	471	862	290	20
10-25	1	0	33	264	879	566	47
25-50	0	0	0	18	47	122	33
50-	0	0	0	0	0	0	0

Table 14: **Observations 00 UTC, August 1997 to July 1999**

$\frac{obs}{for}$	0-0.4	0.4-1	1-5	5-10	10-25	25-50	50-
0-0.4	39	31	174	162	120	30	4
0.4-1	28	27	168	107	99	57	7
1-5	124	100	1155	1044	1110	401	31
5-10	66	23	402	694	1379	534	26
10-25	8	5	75	478	2472	1033	47
25-50	0	0	1	19	479	424	31
50-	0	0	0	0	1	1	0

Table 15: **Observations 03 UTC, August 1997 to July 1999**

$\frac{obs}{for}$	0-0.4	0.4-1	1-5	5-10	10-25	25-50	50-
0-0.4	114	48	313	257	185	79	22
0.4-1	69	28	242	158	142	53	17
1-5	357	125	1279	1308	1423	507	35
5-10	217	25	279	680	1384	429	26
10-25	120	4	58	298	1981	840	32
25-50	30	0	1	12	283	260	16
50-	4	0	0	0	1	1	0

Table 16: **Observations 06 UTC, August 1997 to July 1999**

$\frac{obs}{for}$	0-0.4	0.4-1	1-5	5-10	10-25	25-50	50-
0-0.4	259	82	657	415	230	74	21
0.4-1	114	44	473	325	265	72	7
1-5	576	155	1809	2042	2475	765	67
5-10	297	12	224	821	2088	849	85
10-25	190	1	49	370	1974	1269	164
25-50	80	0	1	11	153	191	45
50-	22	0	0	0	0	0	0

Table 17: **Observations 09 UTC, August 1997 to July 1999**

$\frac{obs}{for}$	0-0.4	0.4-1	1-5	5-10	10-25	25-50	50-
0-0.4	373	90	680	377	203	36	9
0.4-1	141	66	705	461	345	57	5
1-5	815	108	1685	2038	2913	873	65
5-10	428	3	172	850	2249	1324	131
10-25	231	0	32	540	1892	1856	354
25-50	74	0	1	11	78	141	69
50-	21	0	0	0	0	0	0

Table 18: **Observations 12 UTC, August 1997 to July 1999**

$\frac{obs}{for}$	0-0.4	0.4-1	1-5	5-10	10-25	25-50	50-
0-0.4	456	62	630	326	201	28	1
0.4-1	128	47	560	402	378	66	2
1-5	770	70	1513	1891	2926	989	80
5-10	378	2	168	862	2246	1383	179
10-25	204	0	30	590	2220	2279	463
25-50	36	0	0	24	99	231	103
50-	9	0	0	0	0	0	0

Table 19: **Observations 15 UTC, August 1997 to July 1999**

$\frac{obs}{for}$	0-0.4	0.4-1	1-5	5-10	10-25	25-50	50-
0-0.4	506	53	369	201	91	26	1
0.4-1	111	38	370	218	121	22	1
1-5	723	97	1494	1506	1619	334	20
5-10	335	7	268	965	1976	816	73
10-25	202	0	73	950	3403	2848	541
25-50	28	0	2	96	352	671	270
50-	1	0	0	0	0	0	0

Table 20: **Observations 18 UTC, August 1997 to July 1999**

$\frac{obs}{for}$	0-0.4	0.4-1	1-5	5-10	10-25	25-50	50-
0-0.4	563	41	271	189	95	30	1
0.4-1	77	20	222	135	74	29	5
1-5	461	79	1290	1124	1108	236	27
5-10	227	12	345	926	1632	530	48
10-25	92	1	67	667	3469	2214	283
25-50	26	1	4	61	638	997	258
50-	1	0	0	0	0	1	0

Table 21: **Observations 21 UTC, August 1997 to July 1999**

$\frac{obs}{for}$	0-0.4	0.4-1	1-5	5-10	10-25	25-50	50-
0-0.4	615	26	243	153	133	50	10
0.4-1	61	15	171	105	82	40	14
1-5	363	87	1103	1016	1014	403	46
5-10	246	28	449	811	1405	566	50
10-25	101	3	93	584	2923	1443	110
25-50	30	0	1	30	610	543	65
50-	1	0	0	0	0	1	0
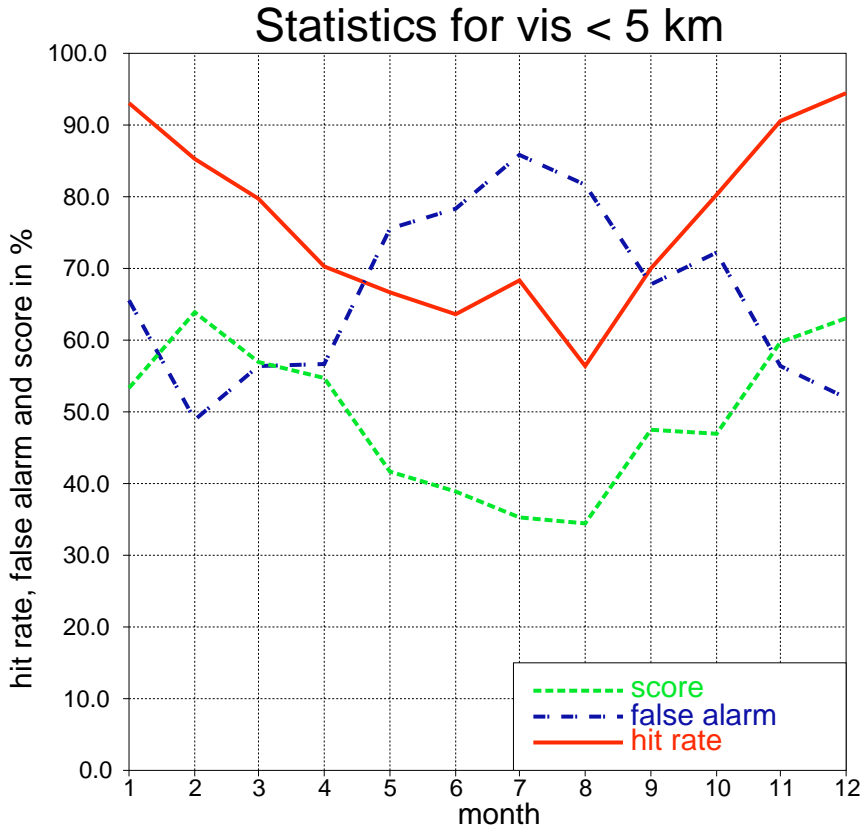
Figure 8: Seasonal variation of hit rate, false alarm and score of visibility based on observed versus diagnosed visibility.

Field data from the tropical Barbados Oceanographic and Meteorological Experiment (BOMEX) has been applied in the test. To obtain a broad range of visibilities an artificial diurnal variation of the sea surface temperature (SST) with an amplitude of $5\,K$ has been introduced. The column version has been run for a period of 24 hours. The results for various model parameters are shown in Figure 9. The subfigure in the left column and 3. row of Figure 9 shows ln(VIS). The diurnal variation in this parameter (resulting mainly from the varying SST) is from 10.6 to 8.1, corresponding to a variation in visibility from about $40\,km$ to $3.3\,km$.

6. A modified visibility function with precipitation intensity included

In the HIRLAM model both rain and snow intensity (in $kg\,m^{-2}s^{-1}$) is calculated every timestep. It is therefore possible to calculate their effect on visibility directly, by applying equation (3) with $\beta_r = \gamma_r C^{0.75}$ for rain and $\beta_s = \gamma_s C^{0.78}$ for snow, as suggested by (Kunkel, 1984), i.e. with $\gamma_r = 1.1$ and $\gamma_s = 10.4$. However, it is then necessary to transform precipitation intensity into precipitation density (in $kg\,m^{-3}$). This is done by using

$$C_n = \frac{P_n}{w_n}, \tag{13}$$

where $n = r$ for rain and $n = s$ for snow. P_n is the precipitation intensity and w_n is the fall speed of precipitation particles in m/s.
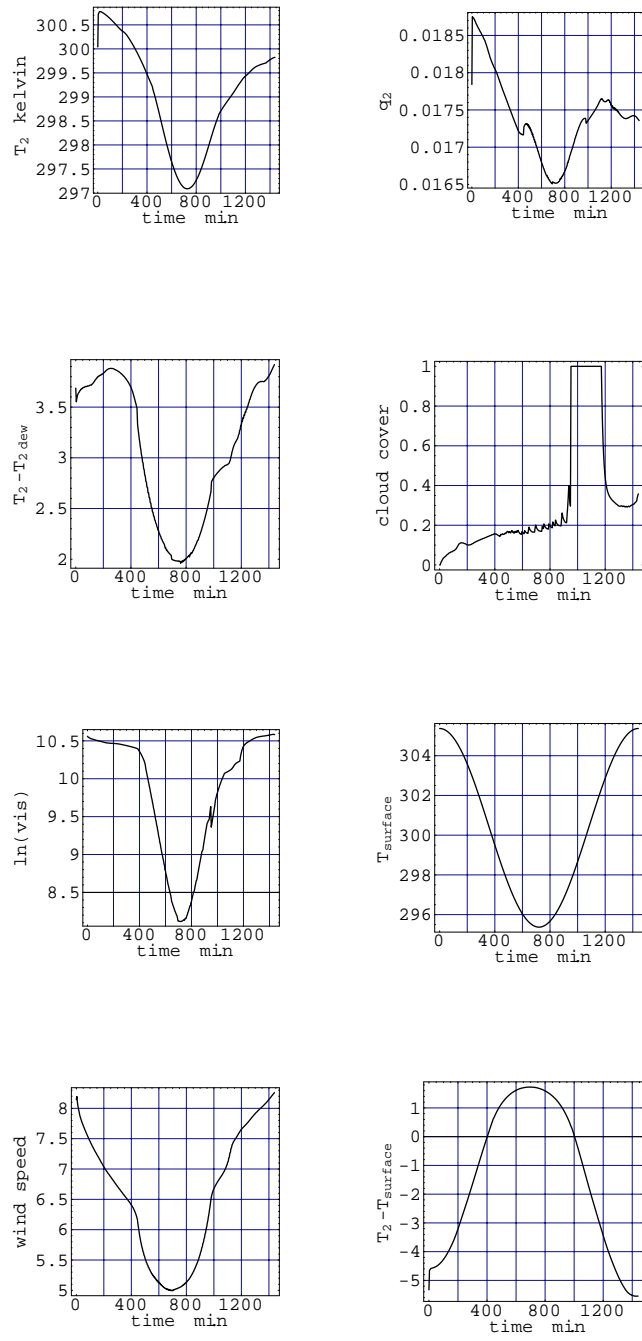
Figure 9: 1D DMI-HIRLAM results based on BOMEX data. For details, see text.

From physical considerations the fall speed is expected to be related to P_n in such a way that large values of P_n are associated with large fall speeds. Furthermore, snow particles are less compact than rain drops. Their 'floating' capability in the air is therefore larger and their fall speeds smaller.

It has so far not been possible to find good data on the relation between P_n and w_n. A simple parameterization has therefore been applied. For rain and snow it is assumed that the fall speed is $w_r = a_r P_r^{1/2}$ and $w_s = a_s P_s^{1/4}$, respectively. Then from (13)

$$C_r = \frac{1}{a_r} \cdot P_r^{1/2} \tag{14}$$

and

$$C_s = \frac{1}{a_s} \cdot P_s^{3/4}, \tag{15}$$

where a_r and a_s are constants with values $a_r = 0.1 \, \mathrm{m^4 \, g^{-1} \, s^{-1}}$ and $a_s = 0.2 a_r$. Note that these units for a_r and a_s gives C_r and C_s in $\mathrm{g \, m^{-3}}$ as in equation (4). Formally the visibility due to rain can be written.

$$VIS_r = d \cdot \sigma_r^{-0.88}, \tag{16}$$

where

$$\sigma_r = \left(\frac{\gamma_r}{\gamma_{cw}} \right)^{1/0.88} \cdot C_r^{0.85} \tag{17}$$

In a similar way the visibility due to snow can be written

$$VIS_s = d \cdot \sigma_s^{-0.88}, \tag{18}$$

with

$$\sigma_r = \left(\frac{\gamma_s}{\gamma_{cw}} \right)^{1/0.88} \cdot C_s^{0.89} \tag{19}$$

Substitution of (14) and (15) into (17) and (19) yields $\sigma_r \simeq 0.03 \cdot P_r^{0.43}$ and $\sigma_s \simeq 1.63 \cdot P_s^{0.67}$. The visibility due to snow and rain as function of precipitation rate in $\mathrm{mm \cdot hour^{-1}}$ using (16) and (18) is shown in Figure 10. It can for example be seen that the visibility at a precipitation rate of about 4 $\mathrm{mm \cdot hour^{-1}}$ drops below 8 ($\ln(8000)=8.99$) and 1 ($\ln(1000)=6.91$) km for rain and snow, respectively.

In the limit of very low precipitation fall speeds the visibility associated with cloud water is accounted for by σ_{cw} in (8). To avoid double counting of σ_{cw} and σ_n ($n = r$ or $n = s$) their combined contribution to the visibility is parameterized by

$$\sigma_t = w_g \cdot \sigma_{cw} + (1 - w_g) \cdot (\sigma_r + \sigma_s). \tag{20}$$

Here $w_g = \exp(-(P_r + P_s)/P_0)$ is a weight function of normalized total precipitation and $P_0 = 1 \cdot 10^{-5} \mathrm{kg \, m^{-2} \, s^{-1}}$.
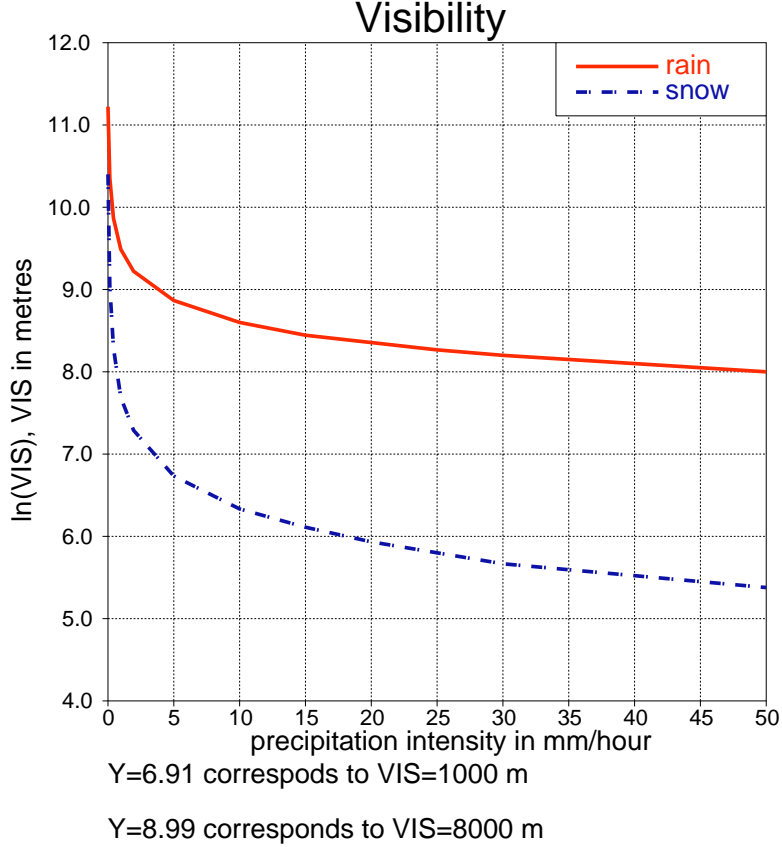
Figure 10: Visibility due to rain and snow as function of precipitation intensity. The ordinate shows ln(VIS).

In the HIRLAM model information about the state of the surface and about the state of the atmosphere at the lowest model level is used to modify the calculation of σ_{cw} in (8). In summary, PCW in (5) now reads

$$PCW = \sigma_{bg} + \sigma_{as} + \sigma_t \tag{21}$$

Over sea $\widehat{dt}$ in (9) is replaced by

$$\widehat{dt}_{sea} = DPD + c_0 + 1 - r_N, \tag{22}$$

where $DPD = T_2 - T_{2d}$ as in (9) and $r_N = q_N/q_N{}^*$ is the relative humidity at the lowest model level (here denoted by subscript N). The superscript * denotes the saturation value of q.

Over land $\widehat{dt}$ is replaced by

$$\widehat{dt}_{land} = \frac{DPD + c_0 + 1 - r_N + (1 - r_2)\left(1 - \frac{q_2{}^*}{q_N{}^*}\right)}{(1 - c_3 \cdot cosz)}, \tag{23}$$

where r_2 is the relative humidity at 2 m height. The use of r_2 and $q_2{}^*$ in place of the surface values r_s and $q_s{}^*$ is an approximation introduced to avoid additional code

21

complexity. The total cloud cover N appearing in (8) is calculated in the model as the maximum-overlap total cloud cover in the column from $p/p_s = 0.9$ to $p/p_s = 0.25$, i.e. very high-level clouds and clouds near the surface are not counted.

7. Three-dimensional DMI-HIRLAM case studies

After the succesfull implementation and test of the visibility code in the column version of DMI-HIRLAM, as described in section 5, the visibility was finally implemented in the 3 dimensional DMI-HIRLAM with the modifications described in section 6 included. The quality of the visibility parameterization was first evaluated on selected cases. Here results from a summer and an autumn case are presented.

All the presented and discussed experiments were done with DMI-HIRLAM version 990110 including the moist process scheme STRACO, the turbulent kinetic energy (TKE) scheme CBR and a modified surface flux parameterization scheme SLFLUX9811 (for more information: see Sass et al., 1999). The model was run with a horizontal resolution of $0.3 \times 0.3°$ and with 31 levels in the vertical on a rotated grid with 110 longitude points and 100 latitude points. The state of the atmosphere at the lateral boundaries was specified by ECMWF analyses and 6 hour forecasts in six hourly steps with linear interpolation in time at intermediate timesteps.

7.1. The June case

In the summer case from June 30, 1997, strong cyclogenesis occurred over the North Sea. This case is interesting, because relatively strong gradients of visibility are present between the two major cold and warm air streams involved in the cyclogenesis. According to the observations in Figure 11 low visibility (from 100 m to a few km) is present in the core of the surface cyclone over the southern part of the North Sea. A band of relatively low visibility is also found west of the cyclone. This band is associated with the occlusion (or bent-back warmfront) of the cyclone.

A 12 hour DMI-HIRLAM forecast (SVB) of visibility at 2 m height (VIS_{2m}) and wind at 10 m height (V_{10m}), valid at 12 UTC, June 30, 1997, is shown in Figure 12. The regions of low visibility in the core of the cyclone and below its bent-back warmfront are clearly present in the forecast, although the forecasted visibility generally is somewhat higher than indicated by the observations. It needs to be mentioned that the observations over the sea are from ships and platforms with an observation height well above 2 m. If low clouds are present these observations may show a visibility that is lower than VIS_{2m}.
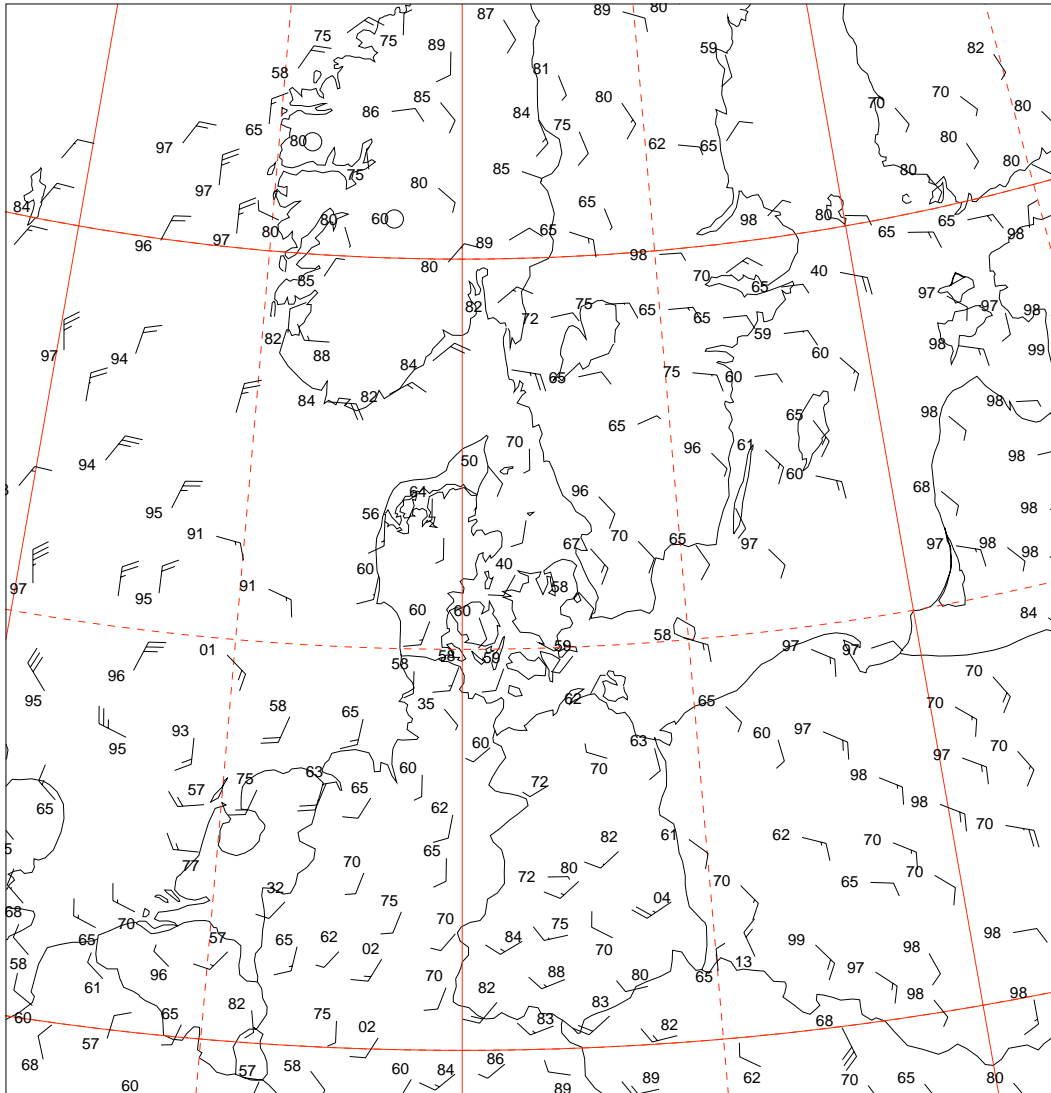
30. juni 1997, 12:00 UTC
Vind, Sigt,

Figure 11: Observed visibility and wind at 10 m height 12 UTC 30 June 1997. Visibility $x < 50\,\mathrm{km}$ is $x/10\,\mathrm{km}$ and $x \geq 50\,\mathrm{km}$ is $x - 50\,\mathrm{km}$. Code numbers from 90 to 99 means: $90(<50\,\mathrm{m})$, $91(50\,\mathrm{m})$, $92(200\,\mathrm{m})$, $93(500\,\mathrm{m})$, $94(1\,\mathrm{km})$, $95(2\,\mathrm{km})$, $96(4\,\mathrm{km})$, $97(10\,\mathrm{km})$, $98(20\,\mathrm{km})$ and $99(\geq 50\,\mathrm{km})$.
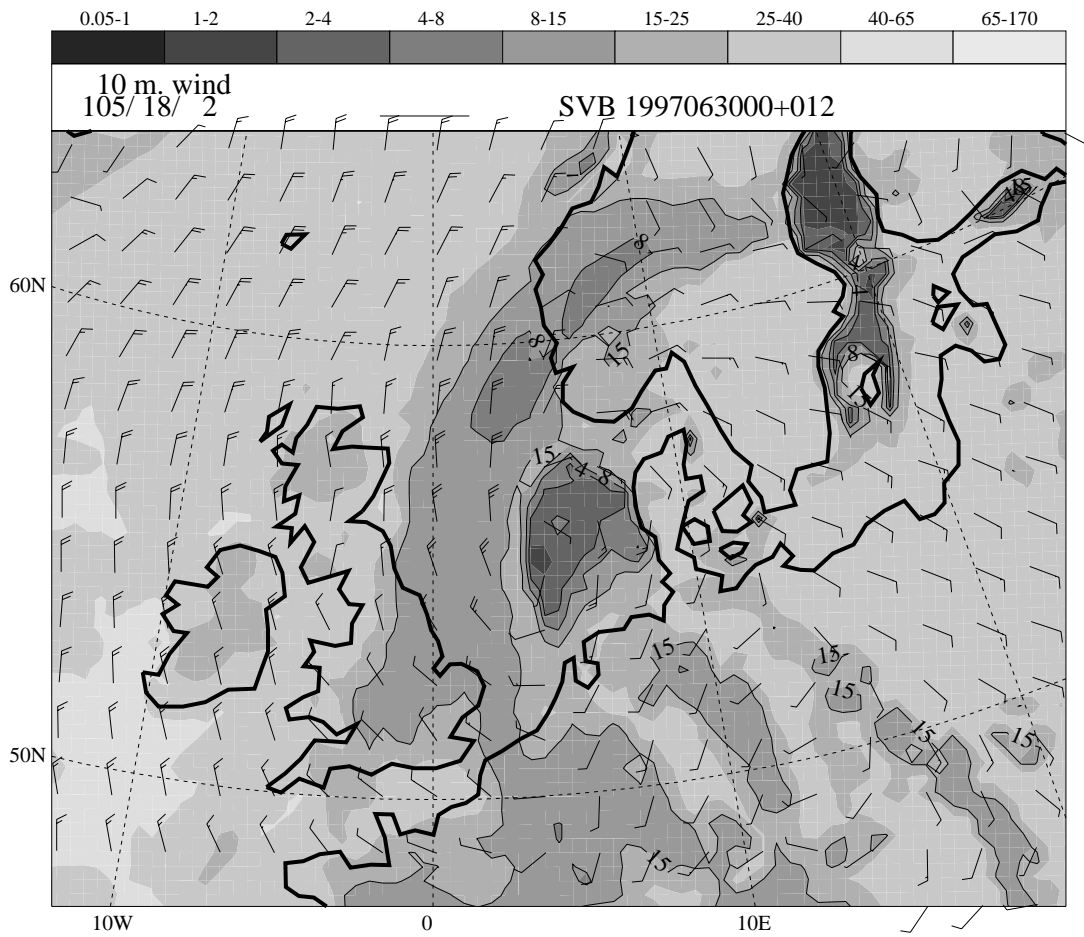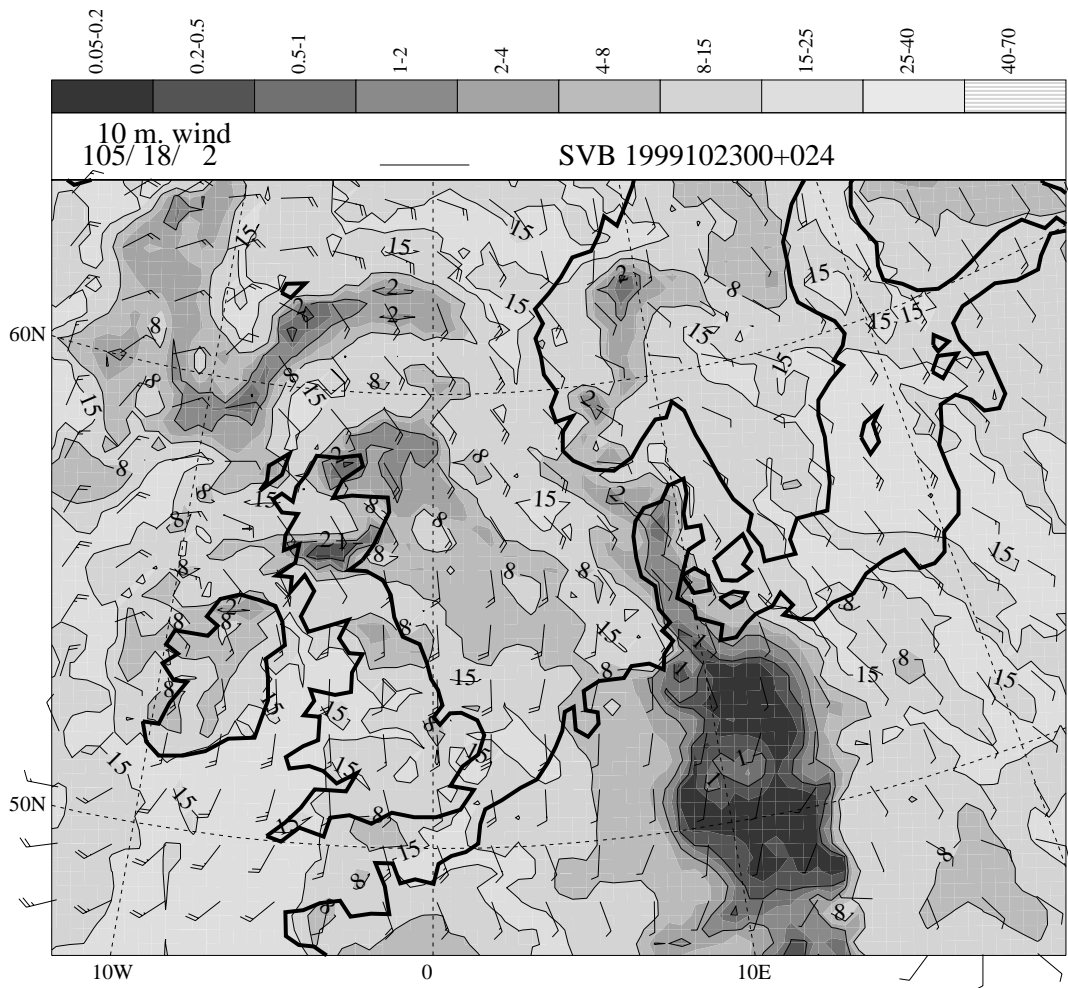
Figure 12: 12 hour forecast of visibility and wind at 10 m height valid 12 UTC 30 June 1997. Shown contours are 4, 8 and 15 km.
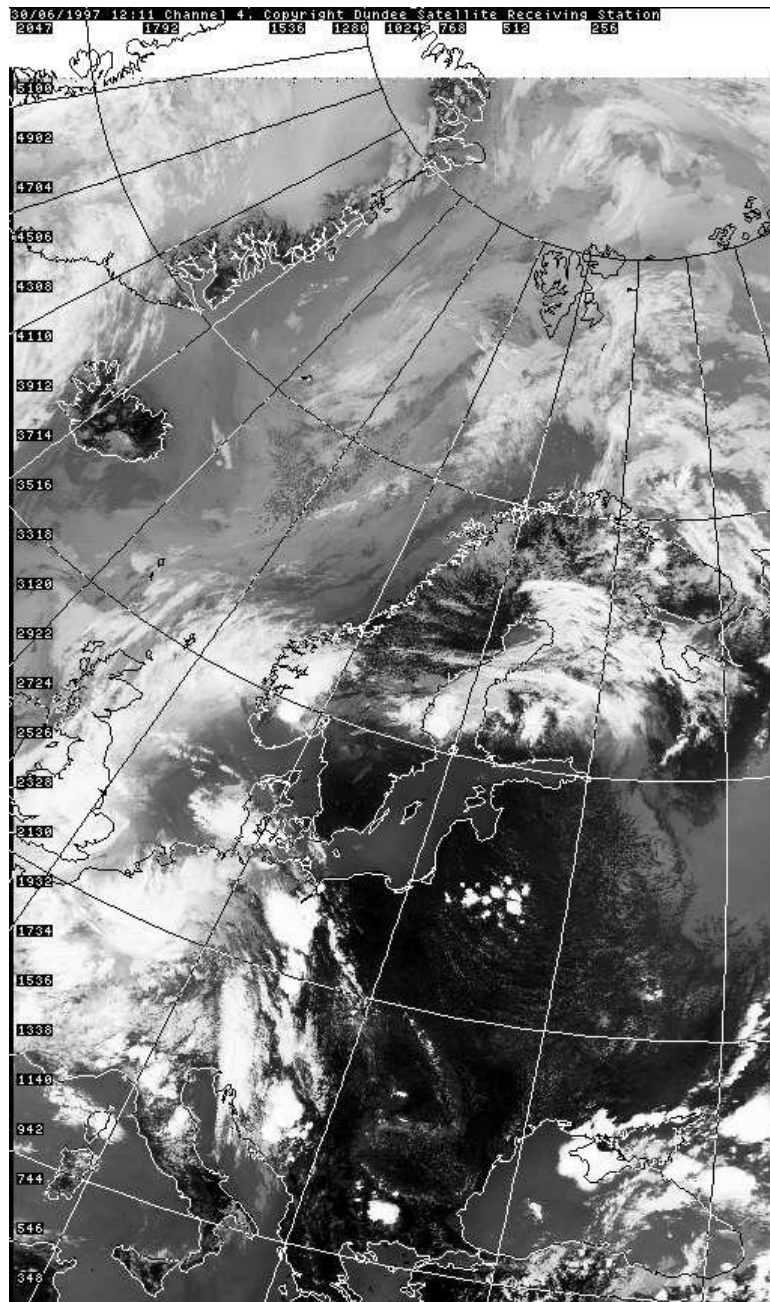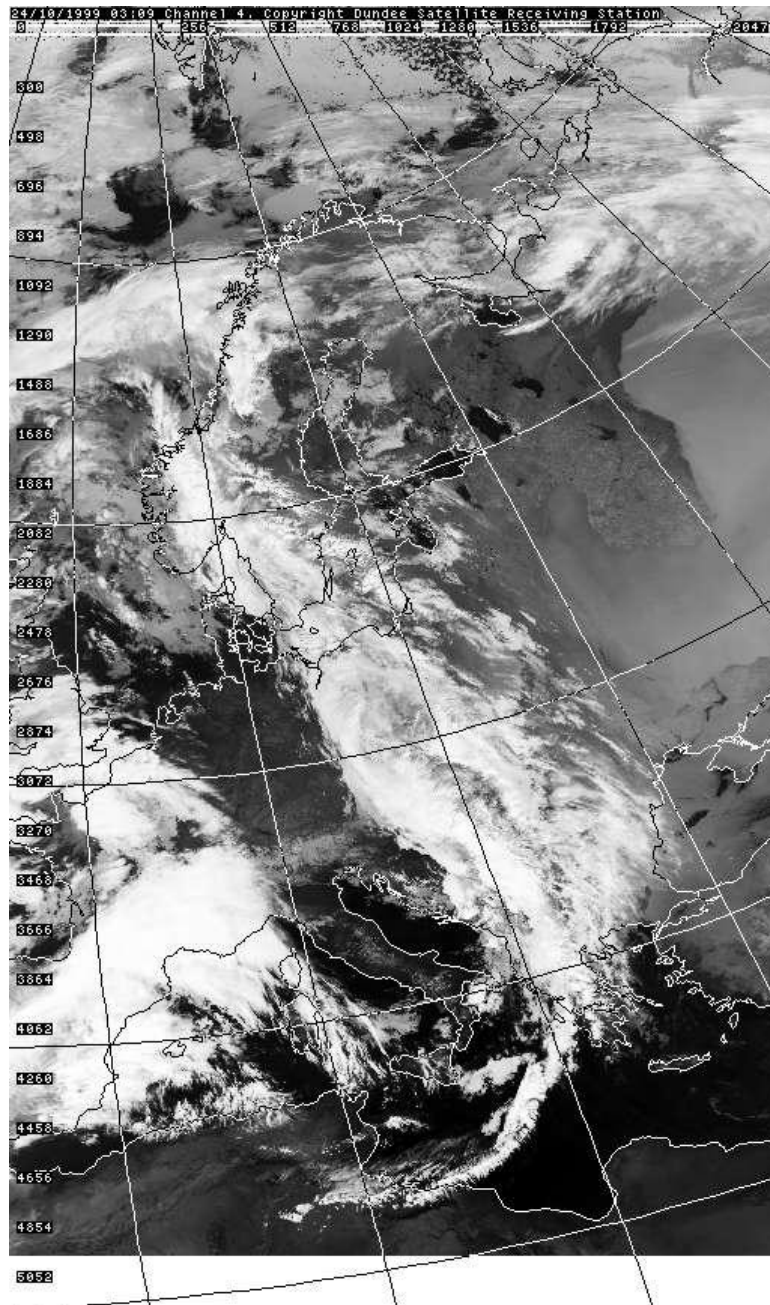
Figure 13: NOAA infrared satellite image from 12.11 UTC 30 June 1997.

Due to lack of sufficient observations the predicted low visibility over parts of the Baltic Sea and over the Gulf of Finland can not be verified by observations. One ship observation with $VIS_{2m} = 4\,$km south of the Åland Islands indicates that the visibility actually is relatively low over this part of the Baltic Sea. The extensive cloud cover over the northern part of the Baltic Sea shown by the NOAA infrared satellite image in Figure 13 is another indication of a possible reduced visibility in this region. It can also be noted that east of the surface cyclone the cloud free regions over land (black in Figure 13) show good coincidence with regions where the predicted visibility is in the range from 25 to 40 km (Figure 12). Closer inspection of the data shows that the predicted visibility nowhere in these regions is above 35 km. Another noteworthy feature is the coincidence between the cloud band along the eastern boundary of the cloudy area over Central Europe seen in Figure 13 and the band of predicted reduced visibility (in the range from 8 to 25 km) over Eastern Europe shown in Figure 12. It is likely that the model rain intensity is responsible for the predicted reduction of visibility.

Later in the afternoon the easterly cloud band seen in Figure 13 spawned a number of severe thunderstorms. Around 18 UTC one of these storms passed central Copenhagen. It developed into the most severe thunderstorm in the Copenhagen area in the 20th century.

7.2. The October case

Around 00 UTC, October 24, 1999 a low from the North Atlantic southwest of Ireland moved across Ireland on a northeastward course. Further east a frontal zone on the western flank of a major high over Russia moved slowly east-northeast. The clouds associated with the low and the frontal zone can be clearly seen in the NOAA infrared satellite image in Figure 16. A NOAA image from 18:06, October 23 (not shown) locates the western boundary of the frontal zone in the Wadden Sea and further south (south of 50°N) approximately along 10°E. The difference in the vertical profiles of temperature (T) and dewpoint (T_d) across the frontal zone over Northern Germany is depicted by the soundings from Greifswald (Figure 17) east of the surface front and Bergen (Figure 18) west of the surface front. In addition, the conditions in the modified cooler air over the North Sea well behind the surface front is shown by the sounding in Figure 19. The soundings indicate that fog is present at Bergen but not at Greifswald east of the surface front and not at Ekofisk over the North Sea west of the front. This is confirmed by by the visibility observations from 00UTC, October 24 (Figure 14). The observations show that relatively low visibility (below 5 km) with areas of fog (visibility below 1 km) is present in the frontal zone while the visibility is relatively high (generally above 10 km) west and east of the frontal zone. The predicted visibility (24 hour forecast from 00 UTC, 23 October) shown in Figure 15 is in fairly good agreement with the observations. The sharp surface temperature and dewpoint inversions on the sounding from Bergen (Figure 18) indicate that the fog at this location has been generated by radiative cooling.
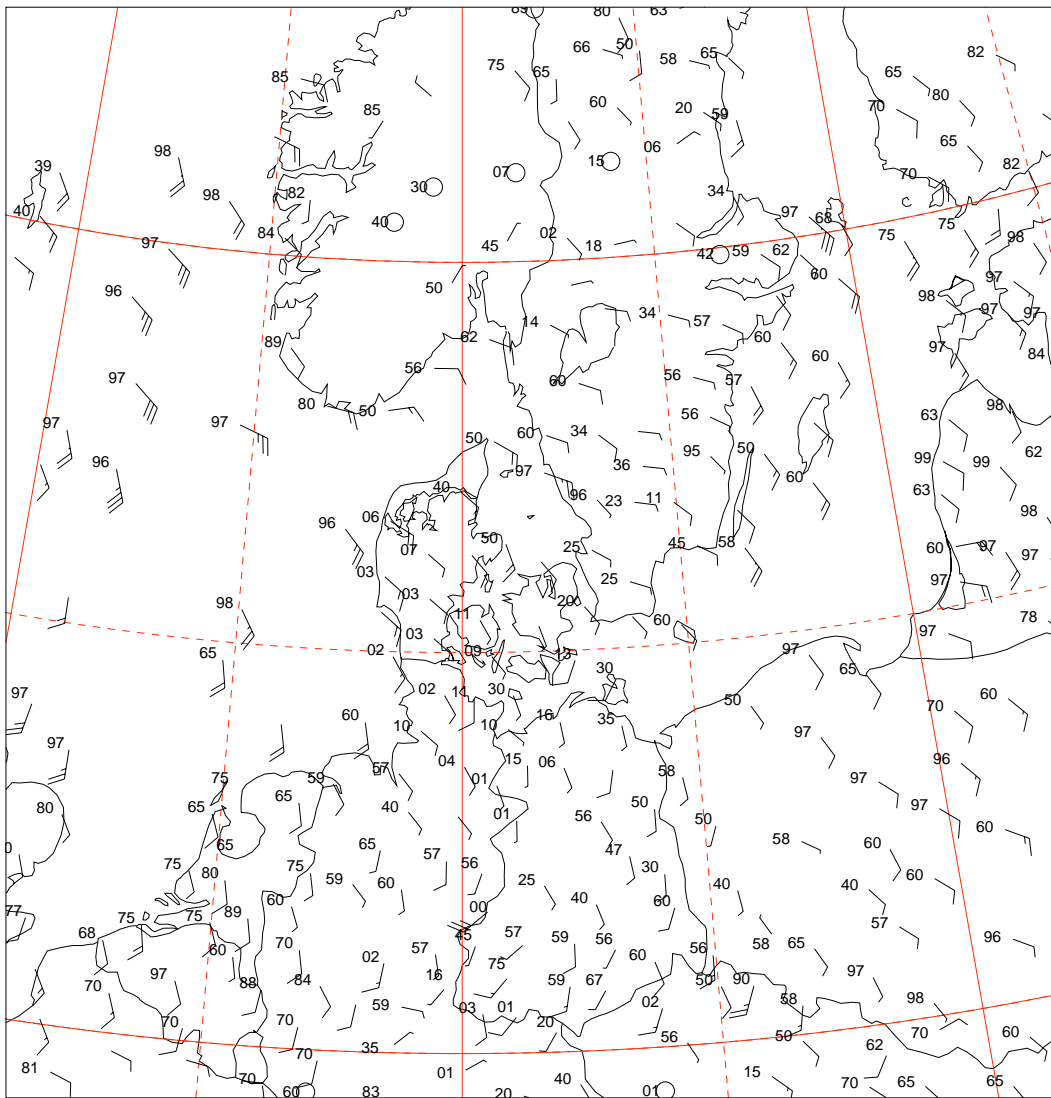
24. oktober 1999, 00:00 UTC
Vind, Sigt,

Figure 14: Observed visibility and wind at $10\,\mathrm{m}$ height 00 UTC 24 October 1999. Visibility $x < 50\,\mathrm{km}$ is $x/10\,\mathrm{km}$ and $x \geq 50\,\mathrm{km}$ is $x - 50\,\mathrm{km}$. Code numbers from 90 to 99 means: $90(<50\,\mathrm{m})$, $91(50\,\mathrm{m})$, $92(200\,\mathrm{m})$, $93(500\,\mathrm{m})$, $94(1\,\mathrm{km})$, $95(2\,\mathrm{km})$, $96(4\,\mathrm{km})$, $97(10\,\mathrm{km})$, $98(20\,\mathrm{km})$ and $99(\geq 50\,\mathrm{km})$.

Figure 15: 24 hours forecast of visibility and wind at 10 m height valid 00 UTC 24 October 1999. Shown contours are 0.5, 2, 8 and 15 km.

Figure 16: NOAA infrared satellite image from 03.09 UTC 24 October 1999.
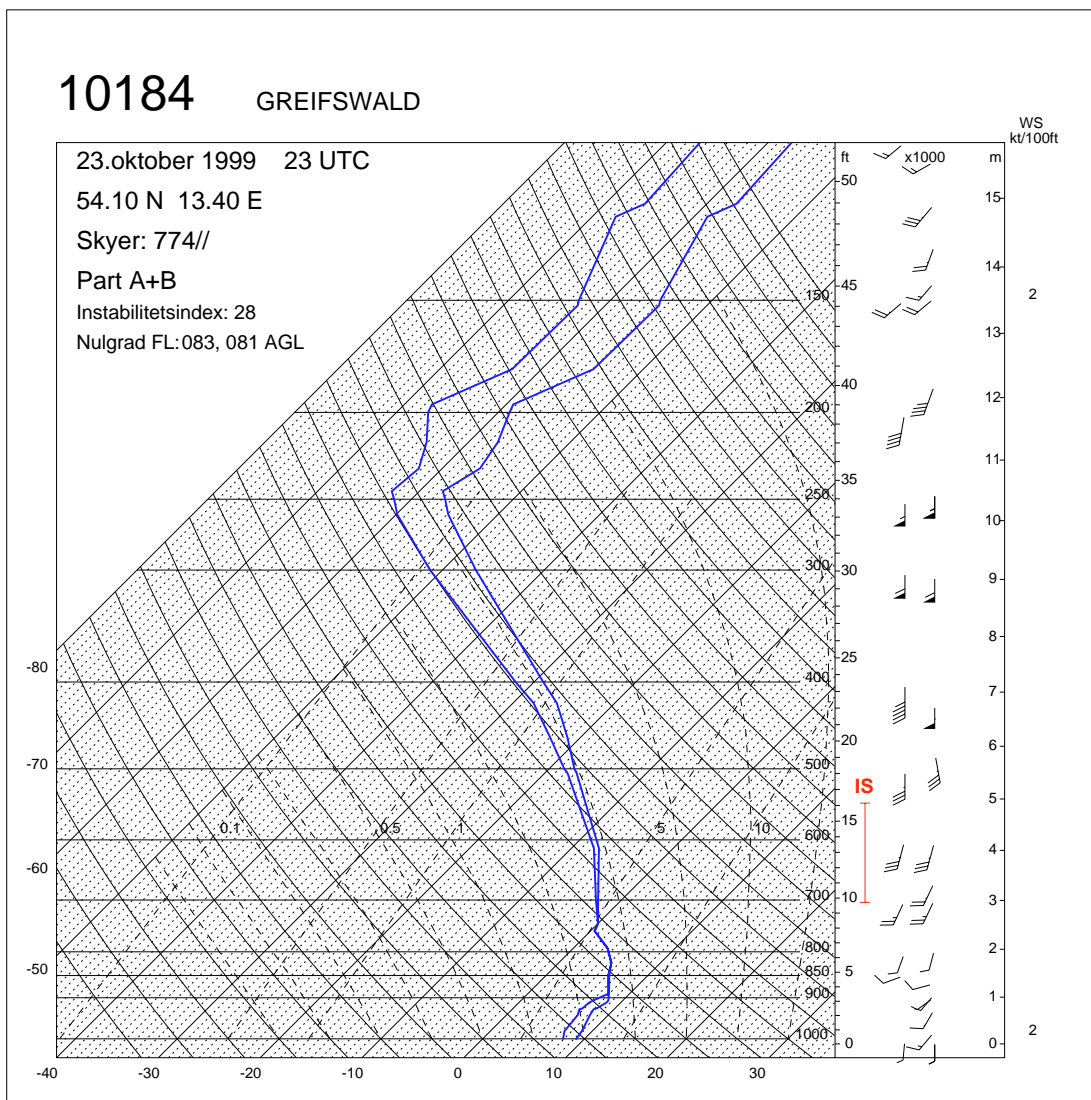
Figure 17: Sounding from Greifswald 23 UTC 23 October 1999.
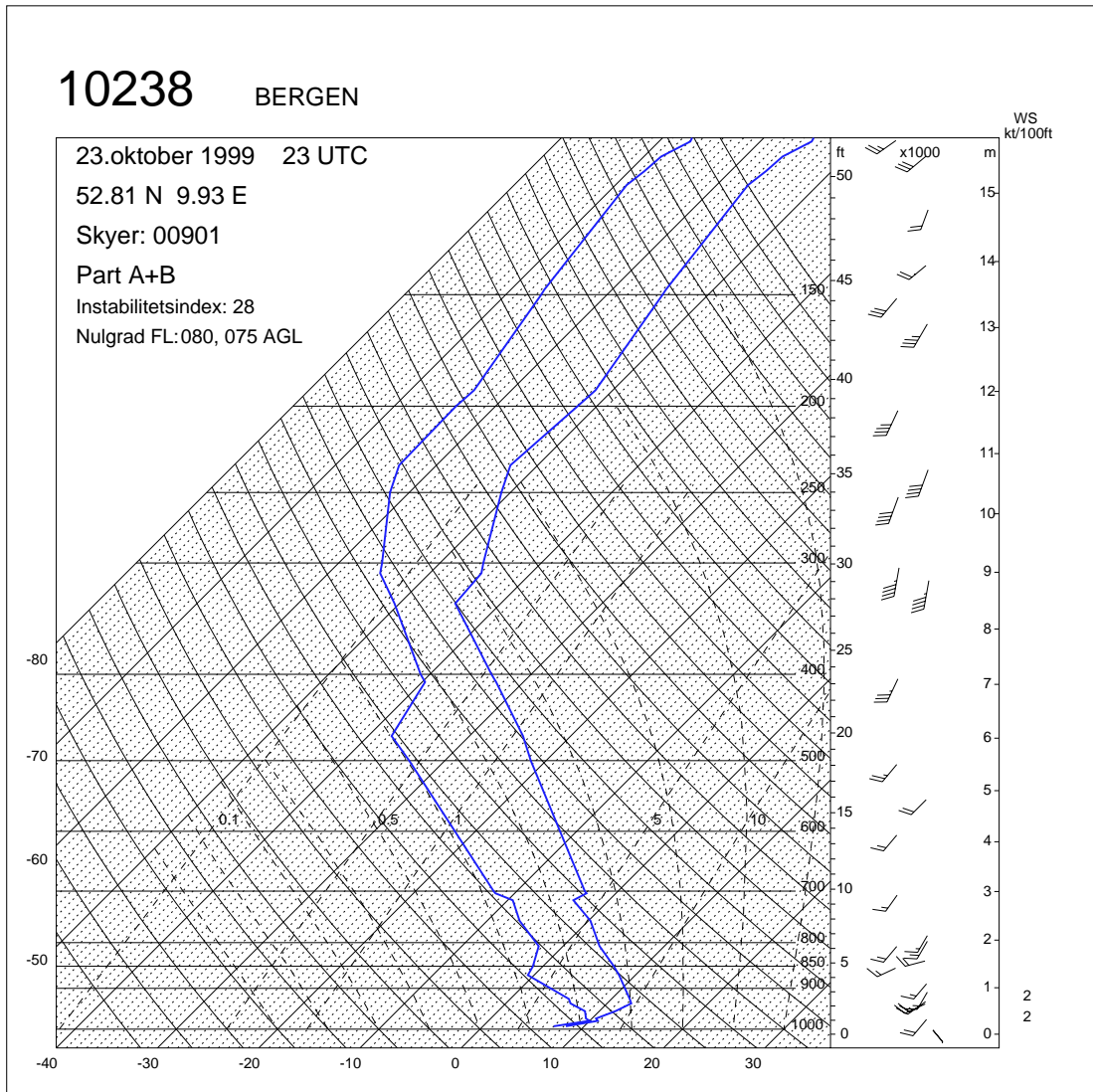
Figure 18: Sounding from Bergen, North Germany, 23 UTC 23 October 1999.
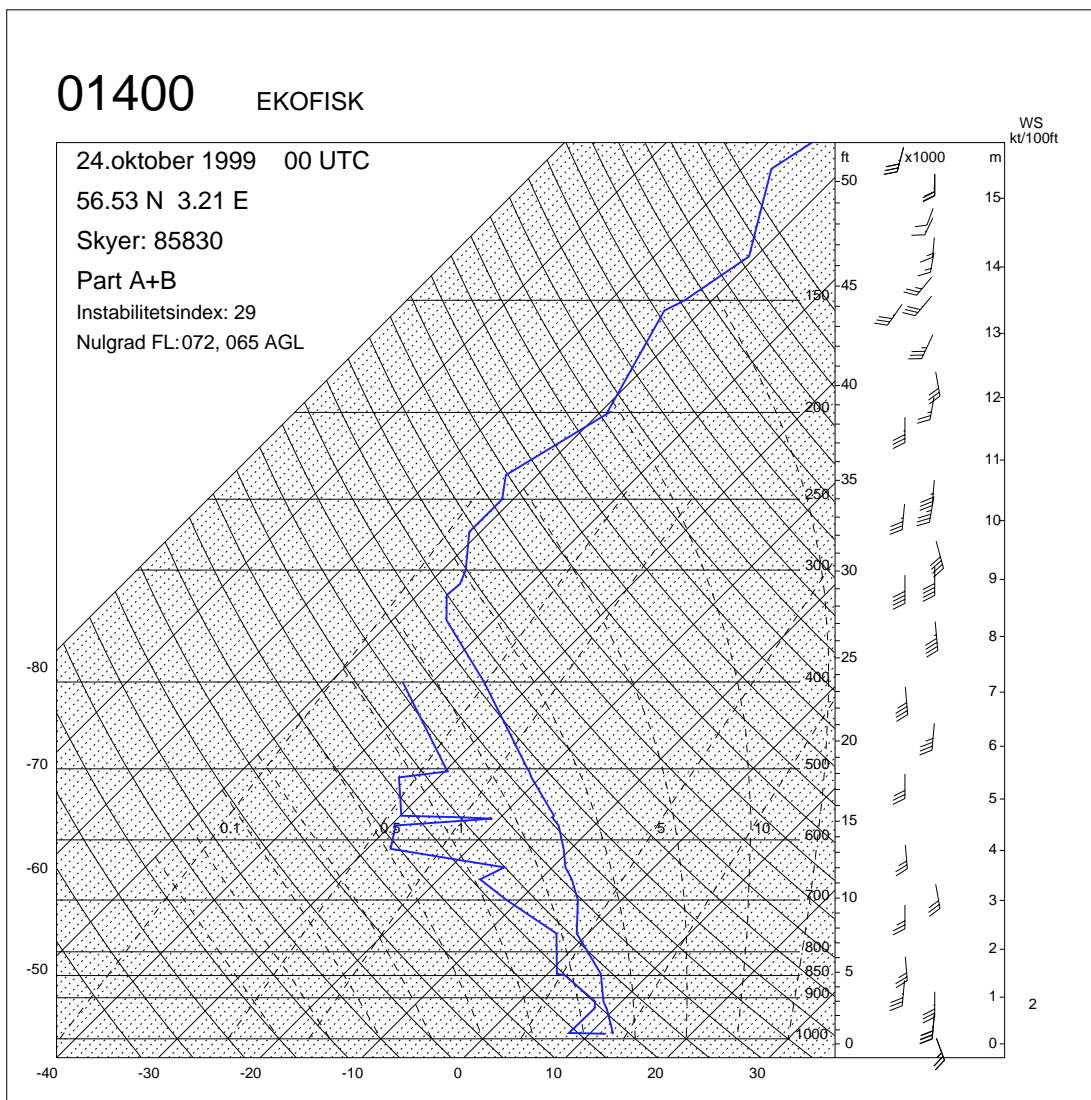
Figure 19: Sounding from Ekofisk , North Sea, 00 UTC 24 October 1999.

8. Obs-verification of visibility

Verification of visibility forecasts against observations (obs-verification) has been done for April, August, November and December 1999. The obs-verification is based on visibility observations from the 29 Danish synop stations shown in Figure 1. The predicted visibility is interpolated to the observation points before intercomparison. For the obs-verification purpose one forecast per day has been run from initial time 00 UTC. For practical reasons the forecast length was limited to 6 hours except for April, where it was extended to 9 hours.

A summary of the obs-verification results are presented in Tables 22 to 34. The Tables 22 to 25 are contingency tables for each month, showing number of observations versus number of forecasts (+03 and +06 hours) in 7 visibility classes. The visibility classes are defined as follows: 1 (0-0.4 km), 2 (0.4-1 km), 3 (1-5 km), 4 (5-10 km), 5 (10-25 km), 6 (25-50 km) and 7 (>50 km). The sum of the numbers in the diagonal gives the number of correct forecasts, i.e. with the observed and predicted visibility within the same class. According to the tables the percentage of correct visibility forecasts for April, August, November and December are respectively 32, 41, 34 and 45%. It is clearly seen that the number of correct forecasts is highest for class 5, 4 and 3. If a one class error in the forecast is accepted the percentage of correct visibility forecasts increases to 69, 81, 74 and 83% for April, August, November and December, respectively. 7% of the visibility forecasts for April have an error larger than two classes. The corresponding numbers for August, November and December are respectively 4, 5 and 4%.

It is in particular difficult to predict low visibility at the correct location and to the correct time as demonstrated for April by Tables 26 to 28. These tables show the hit rate, false alarm and score (see definition in section 4) for class 1, class 1+2 and class 1+2+3.

Table 26 shows that only 0.74% of the visibility observations in class 1 is correct predicted (in space and time) and the false alarm is as high as 92.3%. However, if it is accepted that the class 1 visibility is predicted at a wrong location within a county (approximately 75 km × 75 km) the hit rate increases to 18.5% (Table 27) and the false alarm goes down to 56.5%. If it is also accepted that the predicted class 1 visibility is either 3 hours too early or too late the hit rate increases to 28.1% and the false alarm decreases to 40.0% (Table 28).

Statistically high quality forecasts of visibility means both a high hit rate and a low false alarm, i.e. a high score (a number in the interval from 0 to 1). Tables 26 to 28 shows, as expected, that the score increases significantly from class 1 to class 1+2+3. With the less restrictive conditions valid for Table 28 the score for class 1+2+3 becomes as high as 0.77. With correct timing but not necessarily at the correct location in the county the score is still as high as 0.65 (Table 27).

By definition fog occurs if the visibility is below 1000 m (class 1+2). According to Tables 26 to 28 the scores for prediction of fog in April 1999 were 0.18, 0.37 and 0.55 in the restrictive (Table 26) and the two less restrictive cases (Tables 27 and 28, respectively). For the restrictive case the corresponding numbers for August, November and December are respectively 0.09, 0.34 and 0.30 (Tables 29 to 31). For the less restrictive prediction in space the corresponding numbers are 0.25, 0.71 and 0.56 (tables 32 to 34).

33

Table 22: April. Total number :1604 Hitrate :0.32 One and two class errors: 0.69, 0.93

$\frac{obs}{for}$	0-0.4	0.4-1	1-5	5-10	10-25	25-50	50-
0-0.4	4	6	18	8	14	2	0
0.4-1	9	2	46	27	9	7	0
1-5	30	22	187	133	206	48	3
5-10	7	2	64	72	170	57	3
10-25	4	5	46	65	242	68	5
25-50	0	0	0	2	9	2	0
50-	0	0	0	0	0	0	0

Table 23: August. Total number :1726 Hitrate :0.41 One and two class errors: 0.81, 0.96

$\frac{obs}{for}$	0-0.4	0.4-1	1-5	5-10	10-25	25-50	50-
0-0.4	0	2	6	3	8	3	0
0.4-1	2	0	10	10	6	1	0
1-5	6	5	47	58	112	32	2
5-10	8	5	44	66	149	54	1
10-25	2	8	44	111	570	275	16
25-50	0	0	0	0	36	24	0
50-	0	0	0	0	0	0	0

Table 24: November. Total number :1417 Hitrate :0.34 One and two class errors: 0.74, 0.95

$\frac{obs}{for}$	0-0.4	0.4-1	1-5	5-10	10-25	25-50	50-
0-0.4	16	1	11	11	10	1	0
0.4-1	7	6	19	15	18	3	0
1-5	15	18	68	104	138	21	1
5-10	2	1	57	61	120	28	2
10-25	1	3	64	102	308	132	14
25-50	0	0	2	6	11	18	2
50-	0	0	0	0	0	0	0

Table 25: December. Total number :1551 Hitrate :0.45 One and two class errors: 0.83, 0.96

$\frac{obs}{for}$	0-0.4	0.4-1	1-5	5-10	10-25	25-50	50-
0-0.4	3	3	2	2	7	1	0
0.4-1	1	7	4	3	3	2	0
1-5	12	8	33	30	44	22	0
5-10	2	11	66	94	165	57	5
10-25	6	4	76	160	554	134	7
25-50	0	0	2	3	15	3	0
50-	0	0	0	0	0	0	0

Table 26: April: Comparison of observations with forecasts

	Hitrate	false alarm	score
0-0.4	0.0741	0.9231	0.0755
0-1	0.2308	0.8618	0.1832
0-5	0.7168	0.5851	0.5404

Table 27: April: Comparison of observations with forecasts for each county

	Hitrate	false alarm	score
0-0.4	0.1852	0.5652	0.2988
0-1	0.3407	0.5811	0.3786
0-5	0.8119	0.4514	0.6542

Table 28: April: Observations compared with forecast in the range ± 3 hours

	Hitrate	false alarm	score
0-0.4	0.2812	0.4000	0.4183
0-1	0.5185	0.4043	0.5554
0-5	0.7895	0.2553	0.7660

Table 29: August: Comparison of observations with forecasts

	Hitrate	false alarm	score
0-0.4	0.0000	1.0000	0.0000
0-1	0.1053	0.9216	0.0918
0-5	0.4127	0.7508	0.3260

Table 30: November: Comparison of observations with forecasts

	Hitrate	false alarm	score
0-0.4	0.3902	0.6800	0.3541
0-1	0.4286	0.7458	0.3357
0-5	0.5533	0.6667	0.4325

Table 31: December: Comparison of observations with forecasts

	Hitrate	false alarm	score
0-0.4	0.1250	0.8333	0.1456
0-1	0.2456	0.6316	0.3043
0-5	0.3042	0.6096	0.3459

Table 32: August: Comparison of observations with forecast for the entire county

	Hitrate	false alarm	score
0-0.4	0.1111	0.6000	0.2417
0-1	0.1316	0.6154	0.2474
0-5	0.5397	0.5837	0.4744

Table 33: November: Comparison of observations with forecast for the entire county

	Hitrate	false alarm	score
0-0.4	0.5366	0.3125	0.6048
0-1	0.6857	0.2727	0.7058
0-5	0.6392	0.5327	0.5451

Table 34: December: Comparison of observations with forecast for the entire county

	Hitrate	false alarm	score
0-0.4	0.1667	0.7143	0.2239
0-1	0.4386	0.2647	0.5611
0-5	0.4833	0.2704	0.5876

It can be noted that the scores for August are lower than for the other months. Undoubtly, part of the reason is that fog tends to be more local in summer (mainly radiation fog). It may also contribute that the statistical uncertainty is higher in August due to the relatively few observations of visibility in class 1 and 2 for this month.

9. Summary and discussion

The present report contains a description of an implementation of visibility at 2 m height (VIS_{2m}) as a diagnostic parameter in DMI-HIRLAM. To some extent the diagnostic calculation of visibility is based on a statistical analysis of synop reports from 29 Danish stations covering a continuous period of 2 years. For this reason the derived formula is likely to be optimized for the prevailing meteorological conditions in Denmark. It may be less optimized in for example mountain regions or more generally in a climate deviating significantly from the Danish.

The visibility of air mainly depends on its content of aerosols, cloud water and precipitation particles. In accurate calculations the dependency of the visibility on the droplet size distribution in a fixed amount of cloud water must be considered. As a further complexity, the droplet size distribution depends on the number and properties of aerosols acting as condensation nuclei.

In the DMI-HIRLAM model no information is available about aerosols. The direct effect of aerosols on visibility is therefore calculated in a very simple way. Its indirect effect on visibility through its impact on the cloud water droplet size distribution has not been taken into account.

Cloud water (cw) is a prognostic variable in DMI-HIRLAM, calculated at each model level. At the surface cw is set to zero. In principle cw at the lowest model level could be used to diagnose the effect of cw on VIS_{2m}. However, two serious difficulties are encountered. Firstly, there is no theoretically well-based method available which can be used to calculate cw at 2 m height from the models vertical cw profile. Secondly, the current version of DMI-HIRLAM seems systematically to overestimate the amount of cw in the boundary layer. Therefore, direct use of the predicted boundary layer cw in the prediction of VIS_{2m} is likely to give an undesirable high level of false fog alarms. Consequently, at the present stage of development, the parameterization of visibility does not make use of the predicted cw. Instead a pseudo cloud water (pcw) at 2 m height is calculated from model information about solar zenith angle, cloud cover and wind velocity, temperature and specific humidity both at screen level and at the lowest model level.

The impact of precipitation on VIS_{2m} has been taken into account by making use of the model-prediction of rain and snow intensity.

The quality of the predicted visibility has been monitored in individual cases by subjective comparison of the predicted visibility with verifying visibility observations For extended periods of forecasts the predicted visibility has been evaluated by obs-verification involving point by point intercomparison of predicted and observed visibility.

The case studies show that there usually is good correspondence between the predicted and observed visibility patterns. They also show that the spatial variability of the predicted visibility tends to be less than in the observations. The relative coarse horizontal resolution ($0.3° \times 0.3°$) applied in the experimental DMI-HIRLAM version is

36

likely to make a contribution to the lower spatial variability in the predictions.

The obs-verification results generally show the highest scores for the intermediate range of visibilities (i.e. from 10 to 25 km). The scores are low for dense fog (visibility $< 400\,\mathrm{m}$), but much higher for fog (visibility $< 1000\,\mathrm{m}$). The scores for both dense fog and fog are significantly lower in the summer season that in the remaining part of the year. It is likely that the lower frequency of fog and its clear tendency to be more local in summer contributes to the lower scores for this season.

There is reason to believe that running the same model version with higher horizontal and vertical resolution combined with a more detailed and accurate description of surface parameters (first of all soil moisture) would improve on the prediction scores for fog. Despite of this expectation the presented diagnostic formula for VIS_{2m} must be considered as a first version. There is clearly room for improvements. Future work on fog prediction in DMI-HIRLAM could involve improvements in the parameterization of moist processes in the boundary layer, implementation of an analysis scheme for soil moisture and replacement of the present surface scheme with a more advanced scheme, taking into account various land types, vegetation coverage and vegetation evapotranspiration. The former task would breed the ground for making direct use of the predicted cloud water in the fog prediction. The latter two tasks are expected to improve on the models low-level moisture field.

References

Cotton, W. R. and R. A. Anthes (1989) Storm and Cloud Dynamics. *Academic Press*, International Geophysics Series, Vol. 44.

Kunkel (1984). Parameterization of droplet terminal velocity and extinction coefficient in fog models. *J. Climate Appl. Meteor.* **23**, 34–41.

Sass, B. H., N. W. Nielsen, J. U. Jørgensen and B. Amstrup (1999) The operational DMI-HIRLAM system 2nd rev. ed. *Technical Report 99-21*, available from The Danish Met. Institute.

DANISH METEOROLOGICAL INSTITUTE

Scientific Reports

Scientific reports from the Danish Meteorological Institute cover a variety of geophysical fields, i.e. meteorology (including climatology), oceanography, subjects on air and sea pollution, geomagnetism, solar-terrestrial physics, and physics of the middle and upper atmosphere.

Reports in the series within the last five years:

No. 95-1
Peter Stauning and T.J. Rosenberg:
High-Latitude, day-time absorption spike events
1. morphology and occurrence statistics
Not published

No. 95-2
Niels Larsen: Modelling of changes in stratospheric ozone and other trace gases due to the emission changes : CEC Environment Program Contract No. EV5V-CT92-0079. Contribution to the final report

No. 95-3
Niels Larsen, Bjørn Knudsen, Paul Eriksen, Ib Steen Mikkelsen, Signe Bech Andersen and Torben Stockflet Jørgensen: Investigations of ozone, aerosols, and clouds in the arctic stratosphere : CEC Environment Program Contract No. EV5V-CT92-0074. Contribution to the final report

No. 95-4
Per Høeg and Stig Syndergaard: Study of the derivation of atmospheric properties using radio-occultation technique

No. 95-5
Xiao-Ding Yu, **Xiang-Yu Huang** and **Leif Laursen** and Erik Rasmussen: Application of the HIRLAM system in China: heavy rain forecast experiments in Yangtze River Region

No. 95-6
Bent Hansen Sass: A numerical forecasting system for the prediction of slippery roads

No. 95-7
Per Høeg: Proceeding of URSI International Conference, Working Group AFG1 Copenhagen, June 1995. Atmospheric research and applications using observations based on the GPS/GLONASS System
Not published

No. 95-8
Julie D. Pietrzak: A comparison of advection schemes for ocean modelling
No. 96-1

Poul Frich (co-ordinator), H. Alexandersson, J. Ashcroft, B. Dahlström, G.R. Demarée, A. Drebs, A.F.V. van Engelen, E.J. Førland, I. Hanssen-Bauer, R. Heino, T. Jónsson, K. Jonasson, L. Keegan, P.Ø. Nordli, **T. Schmith**, **P. Steffensen**, H. Tuomenvirta, O.E. Tveito: North Atlantic Climatological Dataset (NACD Version 1) - Final report

No. 96-2
Georg Kjærgaard Andreasen: Daily response of high-latitude current systems to solar wind variations: application of robust multiple regression. Methods on Godhavn magnetometer data

No. 96-3
Jacob Woge Nielsen, Karsten Bolding Kristensen, Lonny Hansen: Extreme sea level highs: a statistical tide gauge data study

No. 96-4
Jens Hesselbjerg Christensen, Ole Bøssing Christensen, Philippe Lopez, Erik van Meijgaard, Michael Botzet: The HIRLAM4 Regional Atmospheric Climate Model

No. 96-5
Xiang-Yu Huang: Horizontal diffusion and filtering in a mesoscale numerical weather prediction model

No. 96-6
Henrik Svensmark and Eigil Friis-Christensen: Variation of cosmic ray flux and global cloud coverage - a missing link in solar-climate relationships

No. 96-7
Jens Havskov Sørensen and Christian Ødum Jensen: A computer system for the management of epidemiological data and prediction of risk and economic consequences during outbreaks of foot-and-mouth disease. CEC AIR Programme. Contract No. AIR3 - CT92-0652

No. 96-8
Jens Havskov Sørensen: Quasi-automatic of input for LINCOM and RIMPUFF, and output conversion. CEC AIR Programme. Contract No. AIR3 - CT92-0652

No. 96-9
Rashpal S. Gill and Hans H. Valeur:
Evaluation of the radarsat imagery for the operational mapping of sea ice around Greenland

No. 96-10
Jens Hesselbjerg Christensen, Bennert Machenhauer, Richard G. Jones, Christoph Schär, Paolo Michele Ruti, Manuel Castro and Guido Visconti:
Validation of present-day regional climate simulations over Europe: LAM simulations with observed boundary conditions

No. 96-11
Niels Larsen, Bjørn Knudsen, Paul Eriksen, Ib Steen Mikkelsen, Signe Bech Andersen and Torben Stockflet Jørgensen: European Stratospheric Monitoring Stations in the Artic: An European contribution to the Network for Detection of Stratospheric Change (NDSC): CEC Environment Programme Contract EV5V-CT93-0333: DMI contribution to the final report

No. 96-12
Niels Larsen: Effects of heterogeneous chemistry on the composition of the stratosphere: CEC Environment Programme Contract EV5V-CT93-0349: DMI contribution to the final report

No. 97-1
E. Friis Christensen og C. Skøtt: Contributions from the International Science Team. The Ørsted Mission - a pre-launch compendium

No. 97-2
Alix Rasmussen, Sissi Kiilsholm, Jens Havskov Sørensen, Ib Steen Mikkelsen: Analysis of tropospheric ozone measurements in Greenland: Contract No. EV5V-CT93-0318 (DG 12 DTEE): DMI's contribution to CEC Final Report Arctic Trophospheric Ozone Chemistry ARCTOC

No. 97-3
Peter Thejll: A search for effects of external events on terrestrial atmospheric pressure: cosmic rays

No. 97-4
Peter Thejll: A search for effects of external events on terrestrial atmospheric pressure: sector boundary crossings

No. 97-5
Knud Lassen: Twentieth century retreat of sea-ice in the Greenland Sea

No. 98-1
Niels Woetman Nielsen, Bjarne Amstrup, Jess U. Jørgensen:
HIRLAM 2.5 parallel tests at DMI: sensitivity to type of schemes for turbulence, moist processes and advection

No. 98-2
Per Høeg, Georg Bergeton Larsen, Hans-Henrik Benzon, Stig Syndergaard, Mette Dahl Mortensen: The GPSOS project
Algorithm functional design and analysis of ionosphere, stratosphere and troposphere observations

No. 98-3
Mette Dahl Mortensen, Per Høeg:
Satellite atmosphere profiling retrieval in a nonlinear troposphere
Previously entitled: Limitations induced by Multipath

No. 98-4
Mette Dahl Mortensen, Per Høeg:
Resolution properties in atmospheric profiling with GPS

No. 98-5
R.S. Gill and M. K. Rosengren
Evaluation of the Radarsat imagery for the operational mapping of sea ice around Greenland in 1997

No. 98-6
R.S. Gill, H.H. Valeur, P. Nielsen and K.Q. Hansen: Using ERS SAR images in the operational mapping of sea ice in the Greenland waters: final report for ESA-ESRIN's: pilot projekt no. PP2.PP2.DK2 and 2nd announcement of opportunity for the exploitation of ERS data projekt No. AO2..DK 102

No. 98-7
Per Høeg et al.: GPS Atmosphere profiling methods and error assessments

No. 98-8
H. Svensmark, N. Woetmann Nielsen and A.M. Sempreviva: Large scale soft and hard turbulent states of the atmosphere

No. 98-9
Philippe Lopez, Eigil Kaas and Annette Guldberg: The full particle-in-cell advection scheme in spherical geometry

No. 00-07
Alix Rasmussen: "Uncertainty of meteorological parameters from DMI-HIRLAM"
(In Press)

No. 00-08
A.L. Morozova: Solar activity and Earth's weather. Effect of the forced atmospheric transparency changes on the troposphere temperature profile studied with atmospheric models

No. 00-09
Niels Larsen, Bjørn M. Knudsen, Michael Gauss, Giovanni Pitari: Effects from high-speed civil traffic aircraft emissions on polar stratospheric clouds

No. 00-10
Søren Andersen: Evaluation of SSM/I sea ice algorithms for use in the SAF on ocean and sea ice, July 2000